ATL-PHYS-2006-003

Single-top s-channel cross-section measurement and sensitivity to a charged higgs boson

A. Lucotte, F. Chevallier

IN2P3 / LPSC - 53, Av. des martyrs, 38026 Grenoble Cedex, France

ATL-PHYS-PUB-2006-014
20 April 2006

Abstract

At the LHC, top quarks are mainly produced via the pair production mechanisms. With a total cross-section of about 835 pb, the LHC will open a new era of precision measurements in top quark physics. Although non-dominant, the single-top production is however far from being negligible with a total cross-section of about a third of the pair production. If a 5σ-evidence of single-top events at the Fermilab $p\bar{p}$ collider is likeliy to occur by the end of the Run II, precise measurements will only be possible at the LHC. They should allow the determination of all three separate contributions to the total single-top cross-section, thus providing valuable tests of the electro-weak top production.

We investigate in this report the possibility to measure the s-channel contribution to the single-top production during the low luminosity running period. A specific analysis based on a topological selection has been developed and is reviewed in detail. The results are presented for an integrated luminosity of 30 fb^{-1} and both statistical sensitivity and systematic uncertainties are assessed.

A precise determination of this contribution constitutes a powerful probe for new physics, this channel being directly sensitive to the presence of an extra charged boson. In the last part of the document, the sensitivity to a charged Higgs boson predicted in a two Higgs Doublet Models of type II has been assessed in the ($\mathrm{m}_{\mathrm{H}^\pm}$ and $\tan\beta$) plane. Results show that this measurement could be one of the main components in charged Higgs boson searches.

Contents

1 Introduction

At the LHC, top quarks are mainly produced via the pair production mechanism. With a total cross-section of about 835 pb [1], the LHC will open a new era of precision measurements in top quark physics. Although non-dominant, the single-top production is however far from being negligible with a total cross-section of about a third of the pair production. If a 5σ-evidence of single-top events at the Fermilab $p\bar{p}$ collider is likeliy to occur by the end of the Run II, precise measurements will only be possible at the LHC. The high statistics should allow the determination of all three contributions to the total single-top cross-section, thus providing valuable tests of the electroweak top production. These measurements should in turn allow the first direct measurement of V_{tb} at the percent level of precision, and will constitute a powerful probe for new physics, via the search for evidence of anomalous couplings to the top quark or via a possible additional contribution to the top production.

This report focusses on the precise determination of the single-top s-channel in the "lepton+jets" channel during a low luminosity run of 30 fb^{-1}. A first approach was defined in early ATLAS publications [2] [3] that will constitute our reference results. The paper is organized as follows: the single-top phenomenology at the LHC is described in Section 2 together with the main Standard Model (SM) background contributions that affect the selection. Section 3 reviews the cross-section measurement, detailling the criteria used to discriminate the signal from backgrounds in a topological selection, as well as the systematic uncertainties affecting the determination. In Section 4 the phenomenology of a 2 Higgs-Doublet Model is reminded and the sensitivity of the single-top s-channel cross-section to the presence of a charged Higgs boson is assessed in the ($m_{H^\pm}$ and $\tan\beta$) plane. Our conclusions are presented in Section 5.

2 Single-top phenomenology at the LHC

This Section presents the mechanisms responsible for the single-top production as well as the main backgrounds affecting the signal selection.

2.1 Single-top production mechanisms

In the Standard Model framework, the single-top production is due to three different mechanisms: the W-boson gluon fusion mode, noted Wg , which includes the t-channel contribution; the associated production of a top quark and a W-boson, noted W+t ; and the s-channel coming from the exchange of a charged boson W*. The corresponding diagrams are shown in Fig. 1. We note however that these definitions are valid only at Leading Order (LO) level of corrections: Next To Leading Order (NLO) calculations may indeed lead to the presence of graphs common to those three mechanisms [4]. The total NLO cross-section for all three mechanisms amounts to about 300 pb at the LHC. Among those channels, the dominant contribution comes from the Wg processes, which account for about 240 pb. The W + t contribution amounts for about 60 pb while the s-channel W* mode is expected with a cross-section of about 10 pb [5][6][7].

In the Standard Model, the top quark almost decays exclusively into a W boson and a b quark. In the following, we use only the leptonic decay of the W's. The s-channel contribution from letponic tau decays has been taken into account and is considered among signal events. For the associated production, we consider the two cases where the leptons originates either directly from the W produced in parallel to the top quark, or from the W-boson appearing in the top quark decay channel. Table 1 reports the cross-sections corresponding to all three mechanisms depending on the charge of the final W-boson.

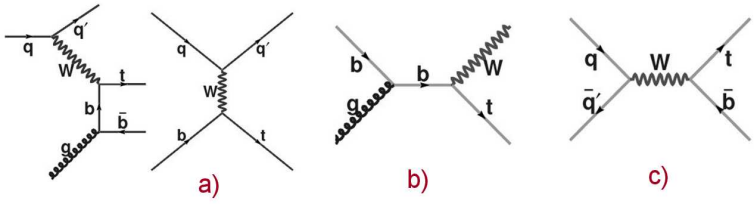

Figure 1: *Main graphs corresponding to the three production mechanisms of single-top events: (a) t-channel (b) associated production (c) s-channel.*

We note that in pp collision, the cross-section for single-top processes are not charge symmetricaly produced: the s-channel $t\bar{b}$ final state cross-section is thus expected to be produced with a factor of 1.60±0.01 higher than the $\bar{t}b$ final state. This ratio amounts to 1.67±0.01 in the t-channel [6]. This feature is of special interest since it generates a charge asymmetry in the leptonic final state that can be exploited in the analysis to reduce the contamination from the top quark pair production, which constitutes the main background to the single-top events selection.

Single-top processes	Cross-section σ (pb)	Theoretical uncertainty PDF	$\mu-$scale	Δm_{top}	$\alpha_s(\delta NLO)$
s-channel					
$W^* \to t\bar{b}$	6.06	$^{+3.3\%}_{-3.9\%}$	±2.0%	$^{+2.3\%}_{-2.0\%}$	±1.2%
$W^* \to \bar{t}b$	3.76	$^{+3.3\%}_{-3.9\%}$	±2.0%	$^{+2.3\%}_{-2.0\%}$	±1.2%
t-channel					
$W \to t\bar{b}q$	150.0	$^{+1.3\%}_{-2.2\%}$	± 3%	$^{+0.8\%}_{-0.7\%}$	±0.1%
$W \to \bar{t}bq$	88.5	$^{+1.3\%}_{-2.2\%}$	± 3%	$^{+0.8\%}_{-0.7\%}$	±0.1%
Associated production					
W + t	32.1	Cteq6			
W + t	34.49	MRST0002			

Table 1: *Contributions of the three individual mechanisms to total the single-top production cross-section [5][6][7] at NLO. Please note that the definition of s-channel, t-channel etc...is valid at the LO only.*

Significant sources of uncertainties affect the theoretical predictions of the production cross-sections: the W* channel is known with a precision of 5.0% at NLO, while the Wg channel has an uncertainty of 3.8%. An uncertainty of 8% is quoted for the W+t channel. Those uncertainties come from three main sources: the uncertainty in the parton luminosity, depending upon the choice of the parton density functions, is particularly important as the b parton or the gluons are involved in the hard processes; the choice for the renormalization and factorization (μ) scales, which accounts for about 2-3% uncertainty in W* and Wg calculations; finally, the uncertainty on the input top quark mass that enters the calculations is significant for the W* channel: a variation from 175 GeV/c^2 to 178 GeV/c^2 of m_t results in a decrease of 6% in the total W* cross-section. An uncertainty of $\pm$4.3 GeV/c^2 in the top mass results in an overall uncertainty of 1 to 3% in the single-top cross-section calculations, depending on the processes.

At the time of the present analysis, only LO single-top generators were available for Monte Carlo studies. We use the TopRex [8] generator for the event production and selection efficiency determination, and normalize a posteriori the event yields to the NLO cross-sections. It is obvious that this approach does not account for the possible biases in final state jet (or lepton) momentum distributions. The use of a NLO generator as MC@NLO [9] appears necessary to validate the selection as it becomes available.

2.2 Standard Model backgrounds

2.2.1 Top pair production

Top pair events constitutes a dscalominant background to single-top productions. The total production cross-section is $\sigma(t\bar{t}) = 835^{+52}_{-39}$ pb [1], about 3 times larger than the corresponding total single-top cross-section, and more than 80 times that of the W* channel.
The main channel affecting the analysis is the "lepton+jets" channel, with a final state composed of two b jets, a high p_T lepton and missing energy; the di-lepton channel ($t\bar{t} \to l\nu bl\nu\bar{b}$) where a high p_T lepton is lost in acceptance also constitute a major background. Finally, top pairs with one or both W decaying into a tau lepton where the τ decays into an electron or a muon, may also survive the selection ($t\bar{t} \to \tau\nu bjjb$ or ($t\bar{t} \to \tau\nu b\tau\nu b$) The corresponding cross-sections are reported in Table 2. Production cross-sections are calculated up to NLO [9].

processes	$\sigma \times$ BR (fb)
$t\bar{t} \to l\nu b$ jjb ($l = e, \mu$)	242,420
$t\bar{t} \to l^+l^-\nu\bar{\nu}b\bar{b}$ ($l = e, \mu$)	38,096
$t\bar{t} \to \tau^+\tau^-\nu\bar{\nu}b\bar{b}$	9,520
$t\bar{t} \to \tau\nu b$ jjb	121,210

Table 2: *Cross-sections convoluted with the Branching Ratio for top pair production used in our analysis.*

Even at NLO, the theoretical uncertainty is dominated by the choice of the renormalization scale: a scale variation of $\mu/2$ to $2 \times \mu$ results in an uncertainty of about 100 pb. Uncertainties due to the choice of the parton density functions, α_s or m_t are much smaller and can be neglected with respect to the latter. As these events constitute our main background, it will therefore be necessary to use cross-section directly from measurements on data to assess properly the contamination of our final sample.

Regarding the Monte Carlo studies carried on $t\bar{t}$ events, we use the (LO) TopRex generator and apply a scale factor on the production cross-sections. Thus, the same remarks as for single-top mechanisms apply here. Further studies including the comparison of TopRex and the NLO generator generator MC@NLO [9] have already started [10].

2.2.2 W+jets and Z+jets production

$WQ\bar{Q}$ events where Q stands for b or c quarks involve the presence of long-lifetime particle jets that are also present in our signal sample. The corresponding cross-section has been computed at LO and is about the same order of magnitude that for the signal. However, NLO calculations [11] are available. They have been performed by imposing some realistic constraints to the partons present in the final state. Numbers together with the requirements applied on the final partons are reported in Table 3 for the various final states.

processes	Cross-sections		
	σ_{NLO} (fb)	σ_{LO} (fb)	Specific requirements
$W^+jj \to e^+\nu jj$	669,000±10	773	$p_T^l \geq 15, p_T^j \geq 20$
$W^-jj \to e^-\nu jj$	491,000±10	558	$p_T^l \geq 15, p_T^j \geq 20$
$Zjj \to e^-e^+jj$	105,000±5	116	$p_T^l \geq 15, p_T^j \geq 20$
$W^+b\bar{b} \to e^+\nu b\bar{b}$	3,060±60	1300	$p_T^l \geq 15, p_T^j \geq 20$
$W^-b\bar{b} \to e^+\nu b\bar{b}$	2,110±50	900	$p_T^l \geq 15, p_T^j \geq 20$
$Zb\bar{b} \to e^+e^-b\bar{b}$	2,280±30	1800	$p_T^l \geq 15, p_T^j \geq 20$

Table 3: *Cross-sections for W+jets and Z+jets events [11].*

As no event generator including NLO calculations is presently available, we use the (LO) TopRex generator for the event production and normalize the corresponding cross-sections to the NLO values. This method imposes us to reproduce the criteria applied in the phenomenological approach [11], in order to normalize properly our selection efficiencies.

W+light jets events constitute a major source of background because of a cross-section several orders of magnitude above the signal. In our case, these processes can mimic the signal if two light jets are wrongly tagged as a b-jet. Some calculations provide the NLO cross-section [11] for specific final states including W+j, W+jj and W+jjj events, with a leptonic decay for the W: in these calculations, requirements that reproduces typical LHC acceptance and energy thresholds

are imposed on leptons and jets composing the final states. To estimate the NLO cross-sections for our selection, we use the same method as for the WQ$\bar{\text{Q}}$ events, reproducing (when possible) the effects of the applied cuts at the parton level. All available generators are presently LO generators and the numbers used for this analysis are quoted in Table 3. Background production makes use of the HERWIG [12] generator for W + jets. The use of more appropriate generators (ALPGEN, AcerMC, MC@NLO) will be needed for future checks.

2.2.3 Di-boson production

Similarly, diboson events with light jets constitute backgrounds to our signal due to the presence a high-p_T lepton as well as b-jets in the final states. The WZ $\rightarrow l\nu b\bar{b}$ production cross-sections have been computed at the NLO level for specific final states including a high-p_T lepton (electron or muon) and is found to be $\sigma \times \text{BR} = 426$ fb [13]. The ZZ $\rightarrow l^-l^+$ $b\bar{b}$ has a cross-section of 340 fb. The WW production where a light jet is mistagged as a b-jet has also to be considered. The corresponding cross-section is 18,500 fb. All those numbers are reported in Table 4. Samples of diboson events have been generated using PYTHIA.

processes	Cross-section $\sigma \times$ BR (fb)
WZ $\rightarrow e^+\nu jj$	430
WW $\rightarrow e^-\nu jj$	18,500
ZZ $\rightarrow l^+l^-\nu jjj$	340

Table 4: *Cross-sections for Standard Model diboson productions.*

2.2.4 QCD background

With a cross-section of about 100 μb the QCD production of pp $\rightarrow b\bar{b}$ is one the main important backgrounds to our signal. In the following we use HERWIG [12] to generate a 10 million sample. Those events constitute a background because due to the presence of two b jets in the final states. The requirements on the presence of a high p_T lepton and high missing energy tend to decrease the contribution. However, given the difference in the cross-section magnitudes, QCD events with a fake lepton and or a bad missing energy reconstruction may pass those requirements. To further reduce this contribution, one can require high thresholds on the b jet p_T , which peak at low values for this background. Section 3.1 shows how the rejection depends on the threshold. Requiring high jet-jet invariant mass and or high total energy may also help to reduce this background to a manageable level.

3 Single-top s-channel cross-section measurement

Our analysis is based on the use of the ATLAS Fast simulation tool [14], which constitutes the only possible way to handle the multi-million event samples required for a low signal efficiency and high-background rejection factor analysis. However, a first comparison with the full simulation has been performed and shows a reasonnable agreement in all the main variables used in the analysis [15]. A thorough comparison between full and fast simulation performance on top pair productions have shown so far a remarkable agreement [17]. A similar approach is being developed for single-top events and will be addressed in a future note.

3.1 Pre-selection

The event selection has been performed in two consecutive stages. A pre-selection stage, which includes the trigger requirements, leads to an event sample with exactly two-b jets, one high p_T lepton and a high missing energy. The statistical sensitivity for this set of criteria is then estimated for two and three-jet final state events. A second stage makes use of the different topologies for signal and backgrounds, and is devoted to purify the pre-defined sample.

3.1.1 Discriminant variables

Following trigger requirements, the pre-selection is based upon the presence of an isolated high-p_T lepton and a high missing transverse energy to reject non-W events. Events with at least two high-p_T jets and at most three jets are selected in order to reduce respectively the inclusive W production as well as the high multiplicity top pair production. Among those high-p_T jets exactly two are required to be identified as coming from the hadronization of a b quark. This allows to reduce significantly QCD and more generally the jet production. Finally, a secondary high p_T lepton veto is applied to reduce both the diboson and dileptonic top pair contaminations.

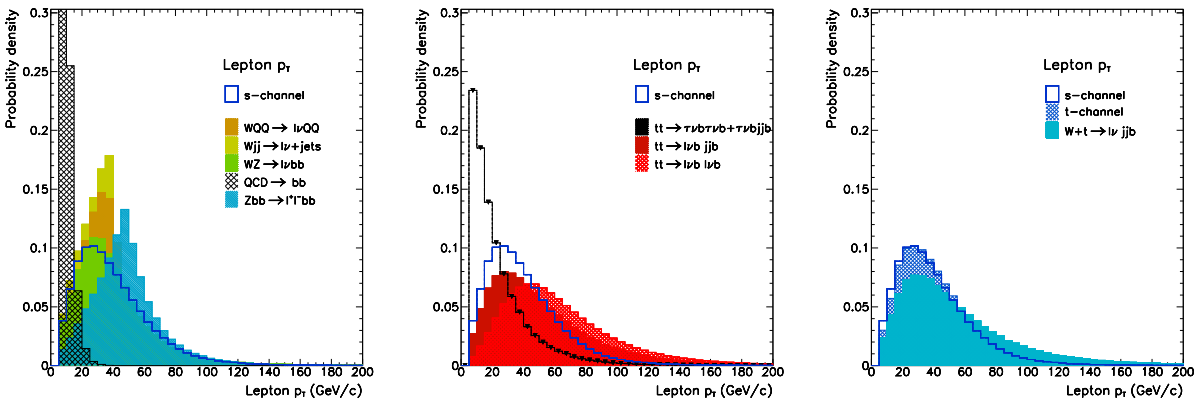

Figure 2: *Lepton transverse momentum probability density for signal and backgrounds.*

Lepton selection

In the ATLAS detector, the electron acceptance is defined in the pseudo-rapidity range $|\eta| \leq 2.5$. Beyond that range, the absence of tracking information makes the lepton identification more complex. The electron transverse energy is determined with a precision of :

$$\sigma(\mathrm{E})/\mathrm{E} = 12\%/\sqrt{\mathrm{E}/\mathrm{GeV}} \oplus 24.5\%/\mathrm{E_T}/\mathrm{GeV} \oplus 0.7\%$$

Fig. 2 displays a comparison of the lepton p_T distribution for single-top events and the different backgrounds. Leptons present in the QCD pp $\rightarrow$ $b\bar{b}$ samples originate mainly from the semi-leptonic decays of b hadrons and are thus much softer than those coming from a W boson decay. Leptons originating from τ decays in $t\bar{t} \rightarrow \tau^+\tau^-\nu\bar{\nu}b\bar{b}$ and $t\bar{t} \rightarrow \tau\nu b$ jjb events also have much lower p_T spectra. All those backgrounds are therefore very sensitive to the lepton p_T threshold used in the analysis. On the upper range of the distribution, W-boson produced leptons tend to be harder in top events than in W+jets events. The average p_T is about 40 GeV/c for the s-channel, 50 GeV/c for $t\bar{t}$ events and has to be compared with the mean value of 30 GeV/c for WZ and $WQ\bar{Q}$ productions. A threshold of 25 GeV/c is set to select a high-p_T lepton. This value corresponds to the lepton trigger threshold that is used to detect such events, and allows to significantly reduce the contamination from non-W as well as tau decays from top pair events.

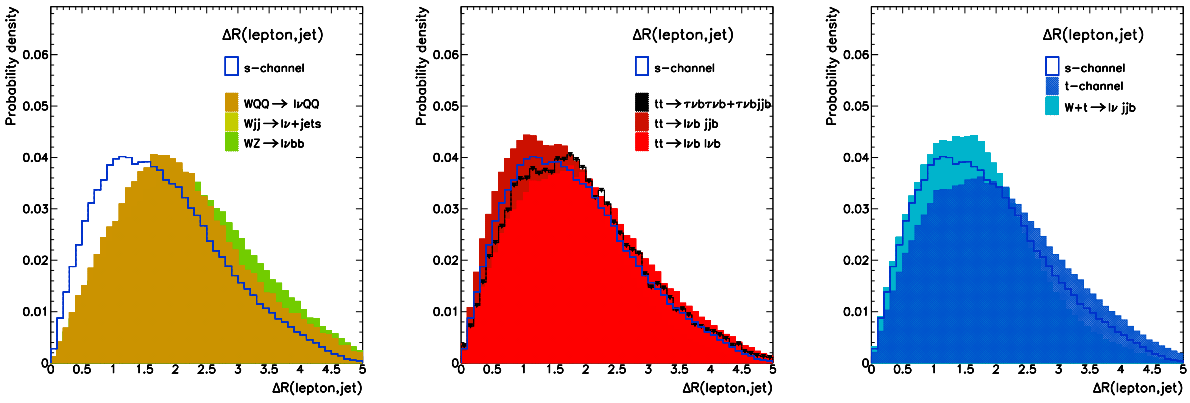

Figure 3: *Lepton isolation probability density for signal and backgrounds. Isolation is defined as the ΔR between the lepton and the closest jet.*

The lepton is required to be isolated. The lepton isolation is defined as the distance to the closest jet by $\Delta\mathrm{R} = \sqrt{\Delta\Phi^2 + \Delta\eta^2}$ and is shown in Fig. 3 for various samples. Note that jets are defined by the use of a cone algorithm whose performance are described in Ref [14]. The isolation of a high-p_T lepton with respect to the closest jet depends upon the topology of events. In a high jet multiplicity environment like $t\bar{t}$ and single top events, the $\Delta\mathrm{R}(\mathrm{lepton,jet})$ value

tend to be lower than in a simple W+jets event. A cut at $\Delta R(\text{lepton}, \text{jet}) \geq 0.4$ is set for the selection.

To remove events with two leptons like $Z \to l^+l^-$ and dileptonic top pairs, a veto is performed in any pairs of leptons with opposite signs and p_T above 10 GeV/c . Note that this lepton veto may introduce some systematic effects due to the mis-identification of the lepton sign as well as a lower lepton identification efficiency at a lower p_T threshold. These effects have to be addressed in a full event reconstruction stage. Note that the sign of the selected lepton provides the nature of the single-top event: a positron or positive muon will sign a $t\bar{b}$ final state, while an electron or muon will sign a $\bar{t}b$ decay.

Missing energy mE_T

The origin of the missing transverse energy observed in the events is due to the undetected neutrino from the W-boson decays. This distribution is shown in Fig. 4 for single-top events and the various backgrounds. Significant differences can be seen in the distributions which carry a significant discriminating power: average values are around 30 GeV/c for W+jets production and about 55 GeV/c for single-top productions; those values are raised above than 60 GeV/c for "lepton+jet" and "dilepton" top pair events. A threshold at 25 GeV/c is thus applied to select a leptonic W decays. The use of the full spectrum may however help the discrimination against backgrounds with softer mE_T like WZ, WQQ, and W+jets events, as well as against events with harder mE_T spectrum like top pairs. A likelihood approach could thus benefit the selection.

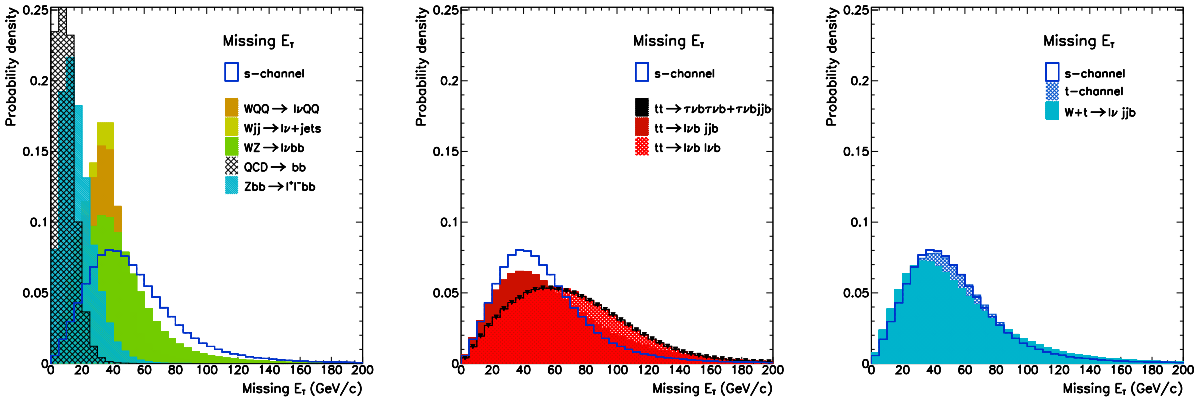

Figure 4: *Transverse missing energy for signal and backgrounds.*

This variable is extremely sensitive to the performance of the hadronic and electromagnetic energy measurement of the detector. Angular and energy resolution, the identification capabilities of noisy calorimeter cells, the modelling of the underlying events and the pile-up effects thus appear as key factors in the missing energy measurement. Again, full reconstruction studies are required to assess the magnitude of those effects.

Light jets

A jet is identified as a group of clusters falling within a fixed cone algorithm defined with a radius of $\Delta R = \sqrt{\Delta\Phi^2 + \Delta\eta^2} = 0.4$. In ATLFAST [14], jets are defined in the pseudo-rapidity range $|\eta| \leq 5.0$ with a p_T above 15 GeV/c . The jet energy resolution is given by:

$$\sigma(E)/E = 50\%/\sqrt{E/GeV} \oplus 3\% \text{ for } |\eta_{jet}| \leq 3$$

$$\sigma(E)/E = 100\%/\sqrt{E/GeV} \oplus 7\% \text{ for } |\eta_{jet}| \geq 3.$$

Distributions for the two highest p_T jets also are shown in Fig. 5 and Fig. 6 respectively. Those Figures show that $t\bar{t}$ events have harder p_T spectra than the other processes, with average values of about 100 GeV/c and 70 GeV/c respectively for the leading and 2nd highest jet energy. Those values are respectively 80 and 50 GeV/c for all three single-top processes. For $WQ\bar{Q}$ and W + jets events, the average energies are found at much lower values, around 35-40 GeV/c for the leading jet and 20-30 GeV/c for the second highest jet energy.

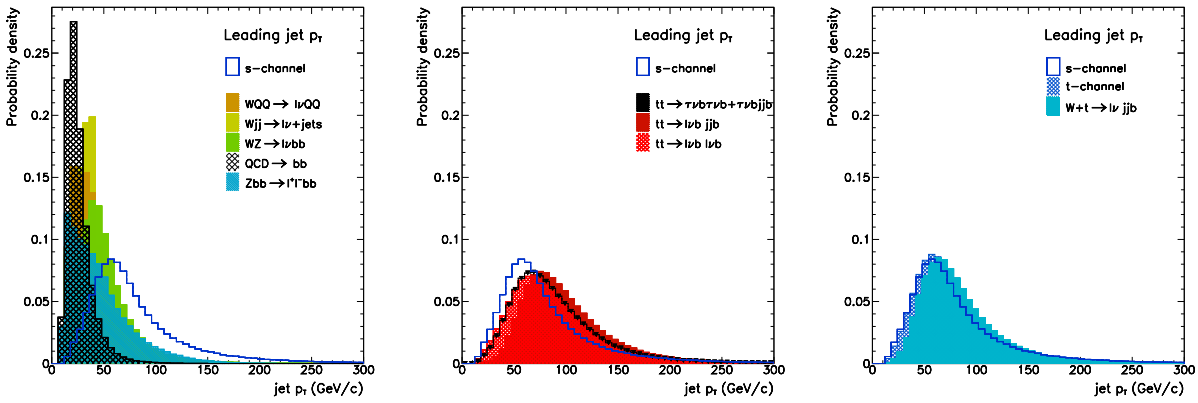

Figure 5: *Transverse momentum for the leading jet for signal and backgrounds.*

The preselection requires at least two jets above a threshold of 25 GeV/c in order to reduce the QCD, W+jets as well as WZ/WW contamination. Again, the use of the full spectrum may revealed useful as an input to a likelihood function.

Jet multiplicity plays a crucial role in discriminating the single-top s-channel from all backgrounds as shown in Fig. 7, where all jets above 15 GeV/c are represented. About 40% single-top s-channel events have exactly two jets and 70% have two or three jets. Jet multiplicity is smaller for both W + jets and $WQ\bar{Q}$ events with only about 30% events reconstructed with more than one jet. On the contrary, more than four jets are expected in the "lepton+jets" and "tau+jets" $t\bar{t}$ events in about 70% of the cases. Significant differences can also be seen among the three

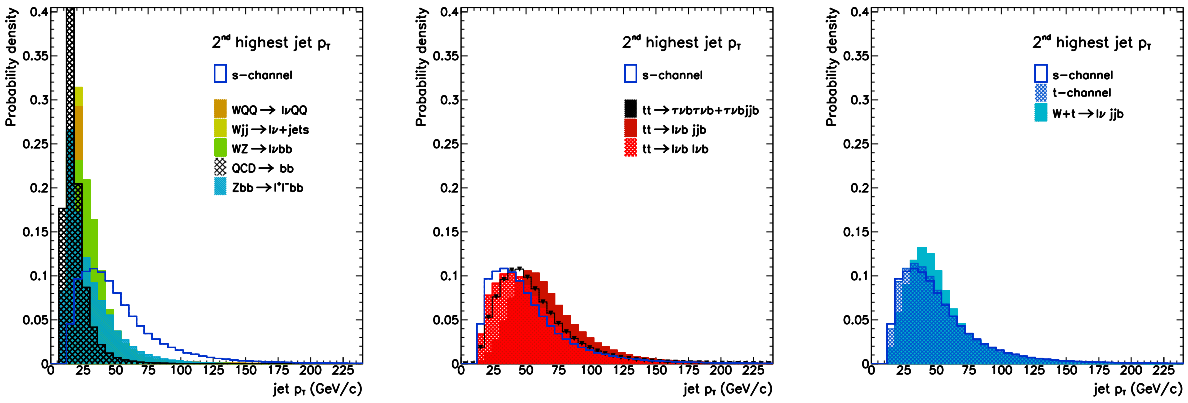

Figure 6: *Transverse momentum for the 2nd highest energy jet for signal and backgrounds.*

single-top production mechanisms. In the associated W + t sample, about 45% of the events have exactly three jets, as expected from the hadronic decay of the W-boson associated to the Top quark. In this sample, about 40% of the events have more than three jets. In the W-gluon process, in addition to the b jet produced in the top quark decay, extra jets may be detected from the other quarks present in the events. It thus appears that the analysis must be performed in bins of jet multiplicity. At the preselection stage, selected events are required to have exactly two or three jets above 15 GeV/c with, among them, at least two above 25 GeV/c . This requirement is crucial to reduce the $t\bar{t}$ contamination level.

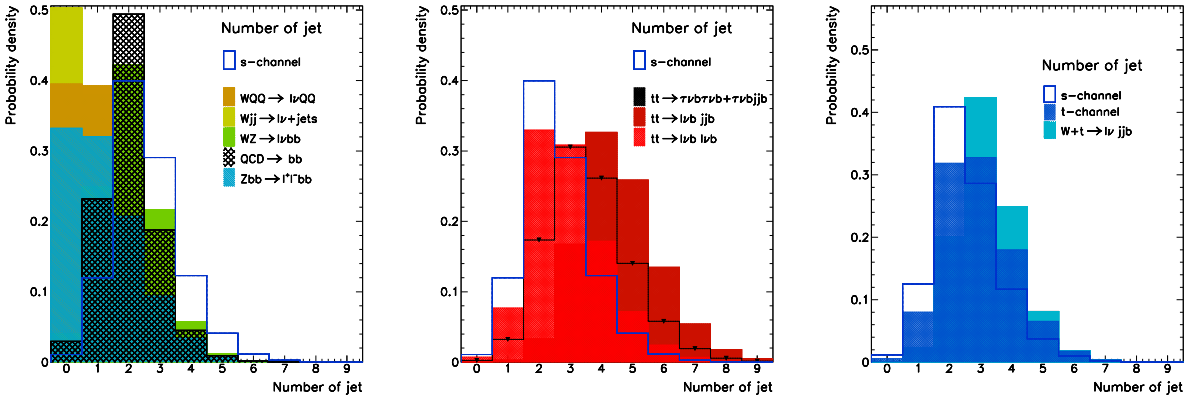

Figure 7: *Number of jets for signal and backgrounds.*

Two issues must be addressed at this stage. The use of NLO generators for both signal and backgrounds may affect significantly those results: it seems mandatory to use them as they become available so as to quantify the effects on selection efficiencies. The second issue concerns the gluon Initial State Radiation (ISR) and Final State Radiation (FSR) modelling and its

impact on the selected jet multiplicity: ISR affect crucially the number of jets that can be selected in the events while FSR have an impact on the jet energy due to the gluon emission in or outside the jet initiated by the parton. The selection efficiency thus depends closely upon the ISR and FSR modelling. These effects are adressed in Section 3.3 devoted to the estimates of the systematic uncertainties affecting the analysis. These two remarks emphasize the role of the jet definition: the choice of a cone algorithm with a larger radius ($\Delta R = 0.7$ for eg.) or the use of a k_T-algorithm to form the jet will affect the result of such analysis.

b-tagged jets

A jet can be identified as a b-jet only in the pseudo-rapidity range $|\eta| \leq 2.5$ corresponding to the tracking acceptance. In ATLFAST [14], the parametrization makes use of a combined tagging efficiency of 60% for b initiated jets above 35 GeV/c in p_T . The corresponding mistag rate is 1% for u,d,s quark jets (factor 100 rejection) and 10% of tagging efficiency for c-quark jets.

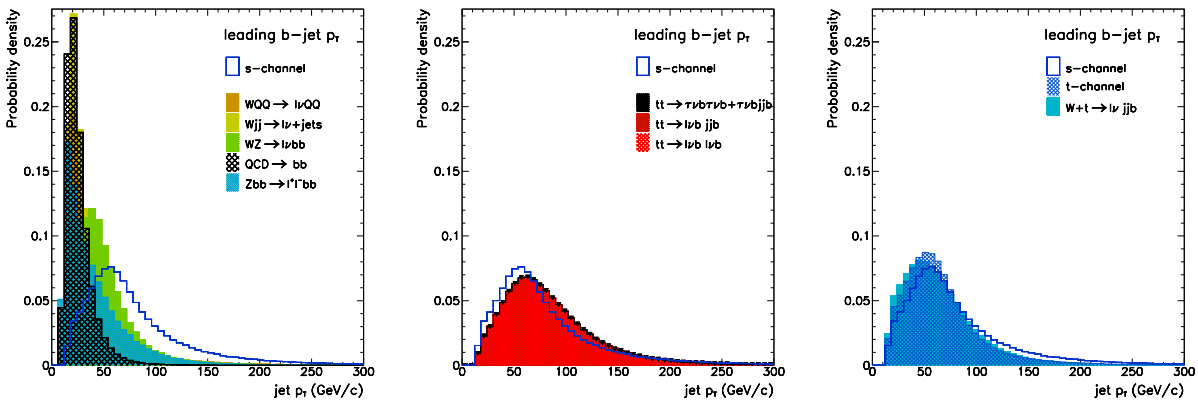

Figure 8: *Leading b-jet transverse momentum for signal and backgrounds.*

Figs. 8 and 9 display the p_T distributions for the two leading b-tagged jets in signal and background events. The average is about 80 GeV/c (resp. 40 GeV/c) for the leading jet (resp. 2nd highest energy b jet). Jets present in QCD pp $\rightarrow b\bar{b}$ events have a significantly softer spectrum than all others sources of backgrounds with an average value well below 30 GeV/c (resp 29 GeV/c). However, the cross-section being several orders of magnitude higher, it is important to set the threshold as high as possible to avoid the contamination from this background. It has been checked that out of 5×10^6 events, 17 events have 1 b-tagged jet (while none pass the 2-btag requirement) for a 30 GeV/c threshold. This number falls to 11 at 40 GeV/c and 7 at 50 GeV/c . This gives confidence that a 35 GeV/c threshold is relevant for our selection. $WQ\bar{Q}$, W+jets and WZ final states are characterized by the presence of softer b-tagged jets than single-top events, with an average p_T of 60 GeV/c for the leading jet and below 30 GeV/c for the 2nd highest energy b jet. A high threshold in the highest b-jet p_T can therefore help reject

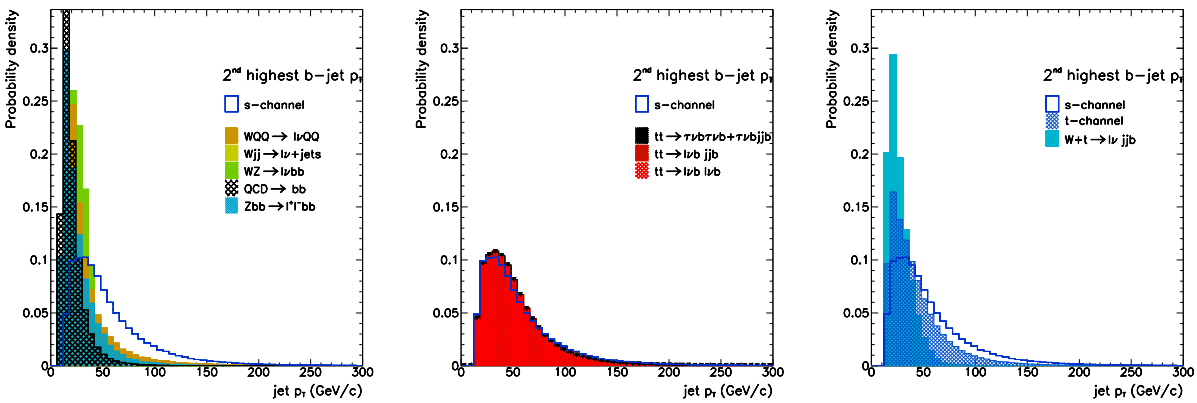

Figure 9: *2nd highest b-jet transverse momentum for signal and backgrounds.*

significantly the QCD and W+jets background. A looser cut may be applied to the 2nd b-jet to further eliminate remaining WQ$\bar{\text{Q}}$ events.

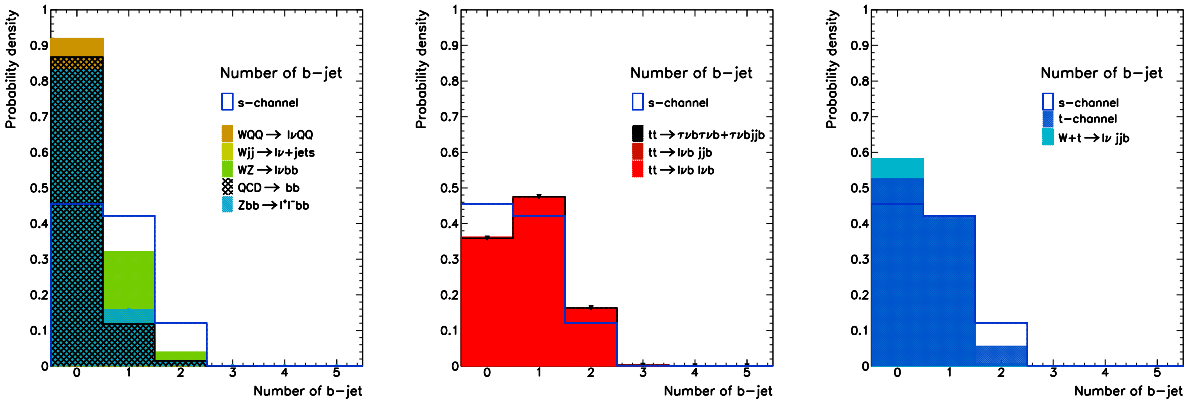

Figure 10: *Number of b-tagged jets for signal and backgrounds.*

The expected number of b-tagged jet is shown in Fig. 10 for signal and all backgrounds. About 90% WQ$\bar{\text{Q}}$ events have only one b-tagged jet, the other being either out of acceptance or below the p_T threshold. No QCD events out of 5,000,000 pass the requirement on two b-tagged jets. The situation is dramatically different in $t\bar{t}$ and W^* events which both contain more than 13% events with two b-tagged jets. Requiring more than one b-tagged jet is therefore mandatory to improve the rejection of QCD and W+jets backgrounds. Regarding the two other single-top mechanisms, the number of b-tagged jets is not as high as for the s-channel events. In the Wg channel, the second b jet is missed in a significant fraction of time once the b parton is produced along the beam pipe, mostly outside the tracking acceptance and with a low p_T , as can be seen in Fig. 9. The probability to see a second b-tagged jet in this sample is less than

15%. For W + t events, no second b is expected, which results in more than 97% events with only one b-tag, the remaining 2nd b-tagged jet coming mostly from charm decay.

The b-jet multiplicity strongly depends upon the b-tagging capabilities of the detector. A high efficiency and a low mistag rate will affect the discrimination against non-top background, making an impact in the analysis sensitivity. Section 3.3 will adress the effects of deviations from the nominal expected performance on the systematic uncertainties affecting the selection efficiencies.

3.1.2 Efficiency and statistical sensitivity

Events were selected if they have at least one high-p_T lepton in the central region with a p_T above 25 GeV/c and a total transverse missing energy above 25 GeV/c . The event must pass a secondary lepton veto cut, applied to any lepton above 10 GeV/c with a sign opposite to that of the selected high p_T lepton. Note that the sign of the high p_T lepton is used to determine the "flavour" of the final top and b-quark pair: a positive (negative) charge lepton signs a $t\bar{b}$ ($\bar{t}b$) final state.

processes	$\bar{t}b$ final state		$t\bar{b}$ final state	
	"2b0j"	"2b1j"	"2b0j"	"2b1j"
s-channel	$3.35 \pm 0.02\%$	1.89%	$3.03 \pm 0.02\%$	1.77%
t-channel	$0.21 \pm 0.004\%$	1.25%	$0.19 \pm 0.004\%$	1.31%
Wt-channel	$0.006 \pm 0.005\%$	0.084%	$0.005 \pm 0.005\%$	0.080%
$t\bar{t}$ background				
$tt \to e\nu b$ jjb	$0.061 \pm 0.002\%$	1.21%	$0.061 \pm 0.002\%$	1.21%
$tt \to e\nu b$ $e\nu b$	$0.494 \pm 0.007\%$	1.13%	$0.494 \pm 0.007\%$	1.13%
$tt \to \tau\nu b, \tau\nu b$	$0.257 \pm 0.02\%$	0.43%	$0.257 \pm 0.02\%$	0.43%
$tt \to \tau\nu b, jjb$	$0.004 \pm 0.0006\%$	0.09%	$0.004 \pm 0.0006\%$	0.09%
Z/W+jets background				
WQQ	$0.19 \pm 0.004\%$	0.07%	$0.19 \pm 0.004\%$	0.06%
$Wjj \to e\nu, jj$	$0.008 \pm 0.0008\%$	0.008%	$0.008 \pm 0.0008\%$	0.008%
$WZ \to e\nu, bb$	$1.18 \pm 0.01\%$	0.39%	$1.15 \pm 0.01\%$	0.41%
$Zb\bar{b} \to e^+e^-b\bar{b}$	$0.005 \pm 0.0018\%$	0.009%	$0.005 \pm 0.0018\%$	0.012%

Table 5: *Absolute efficiency for selected events with 2 b-tagged jets for the 2-jet and 3-jet samples. Numbers are shown for single top processes as well as main backgrounds. Uncertainties come from Monte Carlo statistics only.*

The event must have exactly two or three jets above 15 GeV/c . Among those, two must be above 25 GeV/c . Finally, the events are then required to have, among those two or three selected jets, two b tagged jets with a p_T above a threshold of 30 GeV/c . Selected events are thus classified as "2b0j" (2 b-tagged jets and no extra light jet above 15 GeV/c) or as "2b1j" events (2 b-tagged jets plus one extra light jet and no 4th jet above 15 GeV/c). Table 5 reports

the efficiency for those "2b0j" and "2b1j" samples in both $\bar{t}b$ and $t\bar{b}$ final states. Note that the requirement of two b-tagged jets is crucial to reduce the contamination of W+jets events that have a cross-section several orders of magnitude higher that of the signal. To a lesser extent, this is also true for $t\bar{t}$ events since among the 2-jet and 3-jet events, only a few of them have 2 b-tagged jets. Table 6 reports the number of expected events with 30 fb^{-1}. About 1,200 (840) W* events are expected in the $\bar{t}b$ ($t\bar{b}$) final states. The dominant background comes from the top pair production in the dilepton and "lepton+jets" channels, followed by the WQQ contamination. The remaining W+jets contamination is due to the high cross-section for such events, and is expected, at this stage, to be slightly above the signal expectation. The resulting S/B ratio is about 11% (9%) in the $t\bar{b}$ ($t\bar{b}$) final state. It is obvious that the combination of both final states is required to improve the sensitivity.

processes	$t\bar{b}$ final state	$\bar{t}b$ final state
s-channel	$1,200 \pm 7$	840 ± 4
t-channel	$1,860 \pm 35$	$1,120 \pm 20$
W+t channel	≤ 8	≤ 5
$t\bar{t}$ background		
$tt \rightarrow e\nu b$ jjb	$2,220 \pm 75$	$2,220 \pm 75$
$tt \rightarrow e\nu b$ $e\nu b$	$2,790 \pm 40$	$2,790 \pm 40$
$tt \rightarrow \tau\nu b, \tau\nu b$	360 ± 28	360 ± 28
$tt \rightarrow \tau\nu b, jjb$	60 ± 10	60 ± 10
Z/W+jets background		
WQQ	$2,250 \pm 50$	$1,410 \pm 30$
$Wjj \rightarrow e\nu, jj$	$1,710 \pm 170$	$1,260 \pm 120$
$WZ \rightarrow e\nu b\bar{b}$	90 ± 10	60 ± 5
$Zb\bar{b} \rightarrow e^+e^-b\bar{b}$	7 ± 3	7 ± 3

Table 6: *Number of pre-selected events in the "2b0j" sample expected for an integrated luminosity of 30* fb^{-1}. *Uncertainties come from Monte Carlo statistics only.*

For 2-jet samples, the signal efficiency is slightly above 3.0%. No QCD events are selected out of a sample of 5×10^6 events. Top pair events are selected with an efficiency below 0.1% in the "lepton+jets" channel while tau+jets events are almost negligible. On the contrary "dilepton" (including "ditau") top pair events are selected with a higher efficiency ranging from 0.25 to 0.5%. Overall, this results in an almost equal contamination originating from "lepton+jets" and "dilepton" channels, due to the difference in branching ratios. As expected, the $WQ\bar{Q}$ contamination is greatly reduced by a 2-b tag requirement with a 0.2% selection efficiency. At the same time, only 1.2% WW and WZ diboson events are selected. W+jets events are removed due to the presence of non-b softer jets, with a final yield depending upon the mistag rate (equal to 1% in the present analysis).

Regarding the three-jet samples, the signal efficiency is about 1.9%. While the double tag requirement keeps the W + jets contamination relatively low, the signal is swamped in the $t\bar{t}$ background with a much lower S/B below 1%.

Results have been interpreted as a function of the integrated luminosity. The significance, defined as $S/\sqrt{B}$, is shown as a function of the luminosity in Fig. 11 (Fig. 12) for a 2-jet (3-jet) final state. In 2-jet events it is shown that a 5 σ discovery requires about 5 fb^{-1}. The use of the 3-jet samples does not bring any significant improvement since at least 60 $fb^{-1}$are needed to reach the same yields.

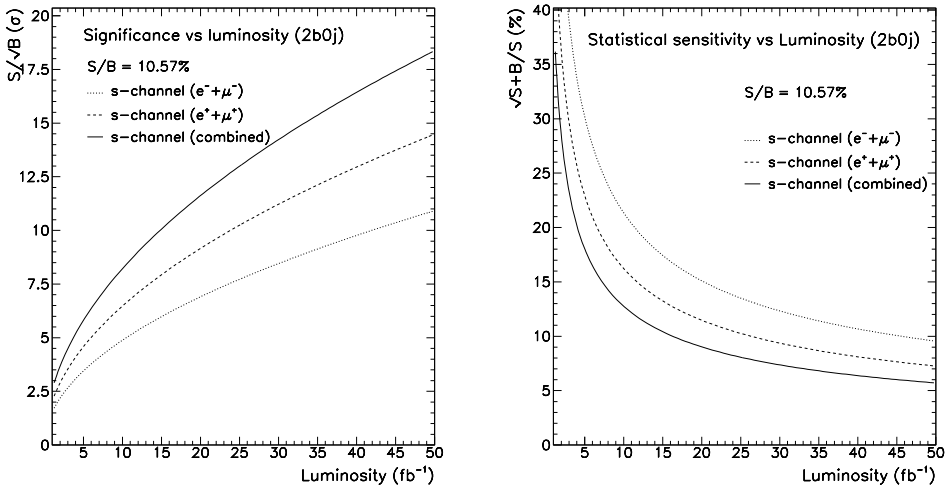

Figure 11: *Signal significance (left) and sensitivity (right) as a function of the integrated luminosity, calculated after the preselection stage.*

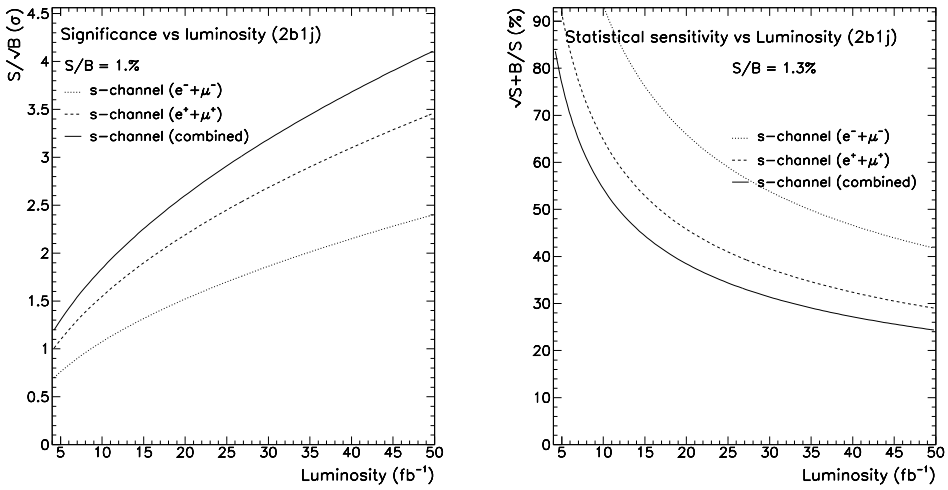

Figure 12: *Signal significance (left) and sensitivity (right) as a function of the integrated luminosity, calculated after the preselection stage.*

The statistical sensitivity to the cross-section measurements has also been evaluated from the ratio $\sqrt{S+B}/S$ which provides the sensitivity of the signal to signal and background statistical fluctuations. Fig. 11 (Fig. 12) displays the statistical sensitivity as a function of the luminosity in the 2-jet (3-jet) sample. It is shown that a sensitivity of 7% can be achieved by combining both $t\bar{b}$ and $\bar{t}b$ final state analyses with an integrated luminosity of 30 fb^{-1}. Corresponding lepton, missing transverse energy and jet momentum distributions are shown in Fig. 13 (Fig. 14) for the $t\bar{b}$ ($\bar{t}b$) final states.

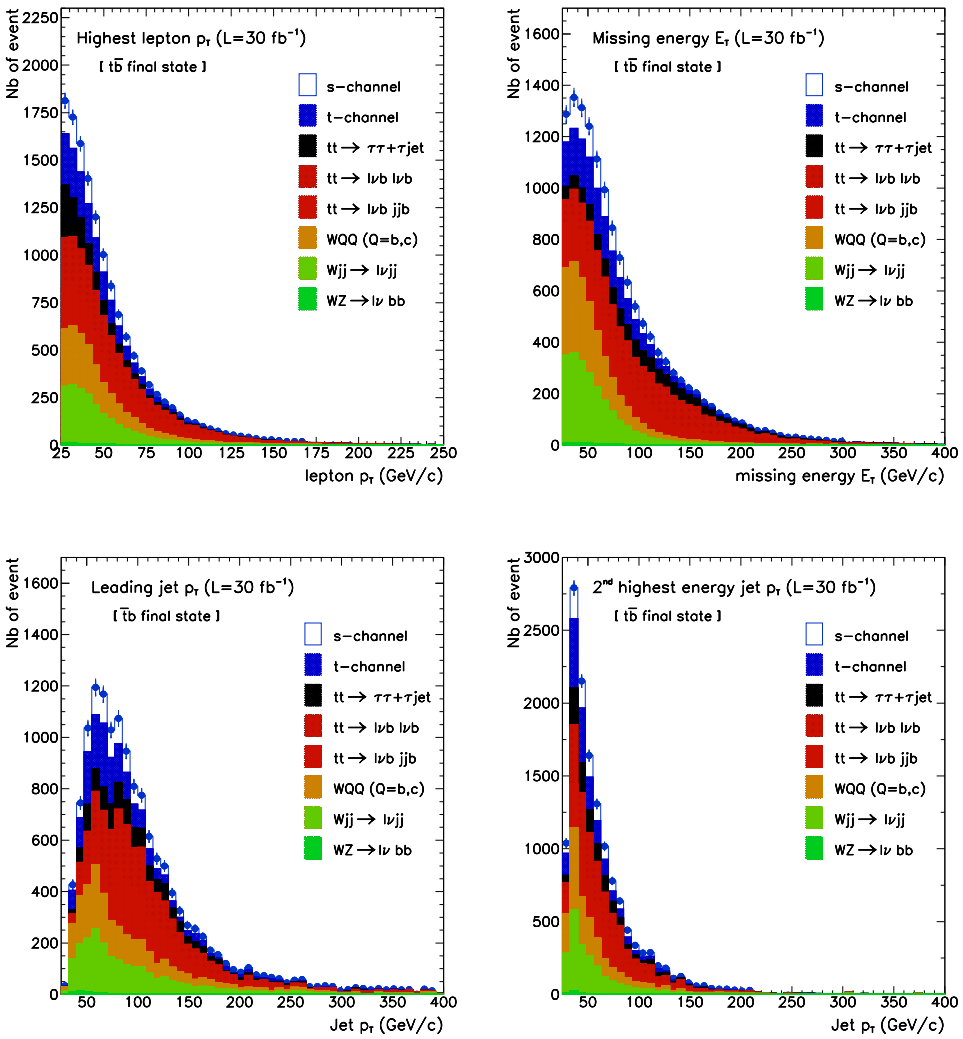

Figure 13: *Distributions for the lepton* p_T *, missing transverse energy, and jets in the* $t\bar{b}$ *final state for a luminosity of 30* fb^{-1}*. The event yields is computed at the preselection stage.*

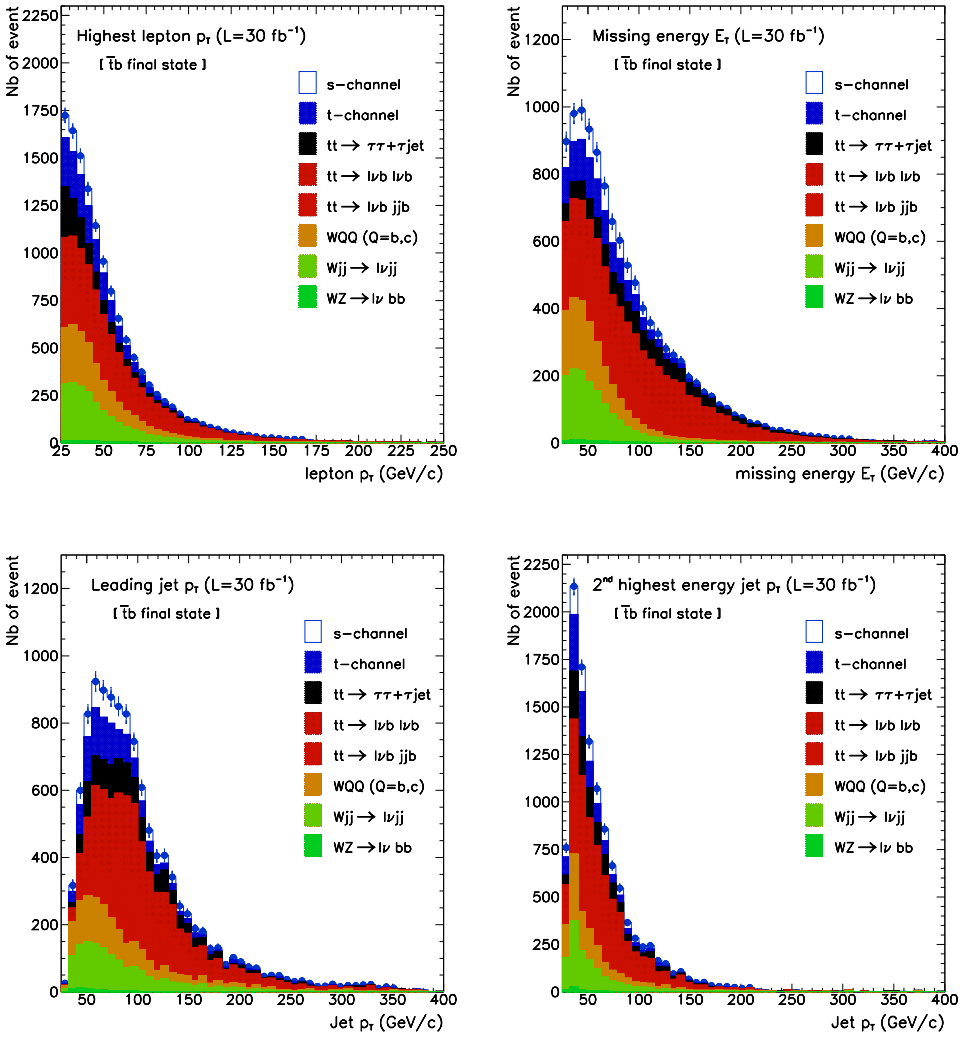

Figure 14: *Distributions for the lepton* p_T *, missing transverse energy, and jets in the* $t\bar{b}$ *final state for a luminosity of 30* fb^{-1}*. The event yields is computed at the preselection stage.*

3.2 Topological selection

After the pre-selection stage, the remaining sample is characterized by a low ratio signal over background. Most of those backgrounds originate from the top pair and $WQ\bar{Q}$ production. In order to purify the sample, we apply additional selection criteria based on topological characteristics: we use the total transverse energy H_T and on the top mass reconstructed from the b jet and the leptonic decays of the W boson.

3.2.1 Total transverse energy H_T

The total transverse energy of the event is shown to have a significant discriminant power against both top pair and W + jets production. While the $t\bar{t}$ events tend to contain harder jets, the latter are characterized by the presence of softer jets in the final state compared to those for the signal. One usually uses the scalar sum of transverse energy computed over jets as well as leptons and missing energy. Obviously this variable is correlated to the number of jets and therefore careful treatment must be applied. In our selection H_T is defined as:

$$H_T = \Sigma_{jet}\ E_T^{jet} + E_T^l + mE_T.$$

The probability density distribution for this quantity is represented in Fig. 15 for signal and the various backgrounds. The H_T distribution peaks at around 180 GeV/c for $WQ\bar{Q}$ events while the average value for the W^* channel is about 230 GeV/c . For $t\bar{t}$ events in the various channels the distributions peak around 300 GeV/c . A window in H_T seems therefore to bring a significant rejection power against both $WQ\bar{Q}$ and $t\bar{t}$ backgrounds.

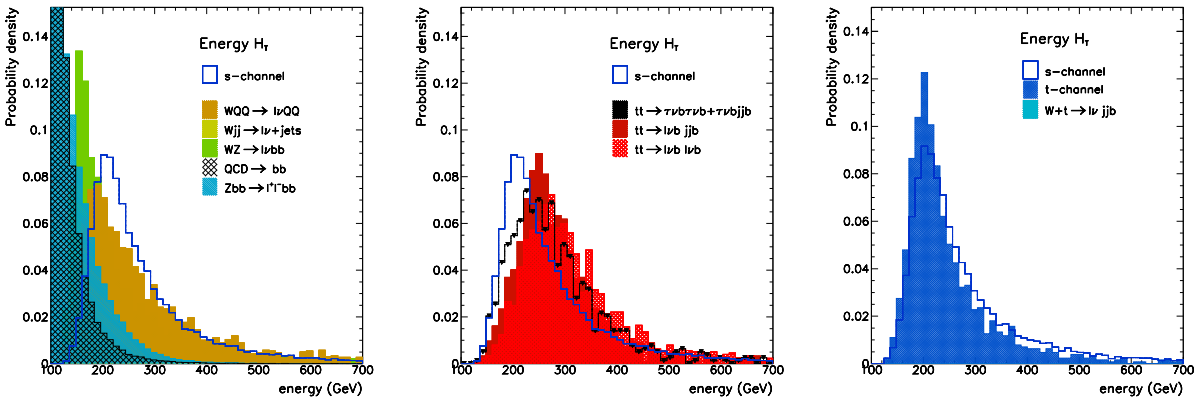

Figure 15: *Distribution of the energy* H_T *for signal and backgrounds.*

Fig. 16 display the event yields after the preselection stage for 30 $fb^{-1}$for both $t\bar{b}$ and $\bar{t}b$ final states. In order to optimize the upper and lower bounds applied on H_T, one can use three estimators: the ratio S/B, which reflects the sample purity as a function the threshold values; the statistical significance $S/\sqrt{B}$; and the sensitivity defined as $S/\sqrt{S+B+\sigma_B}$, which includes

the systematic uncertainty in background estimate, set at $\sigma_B = 12\% \times B$. Fig. 17 show the sensitivity as a function of the H_T energy cut for both the lower and upper bounds.

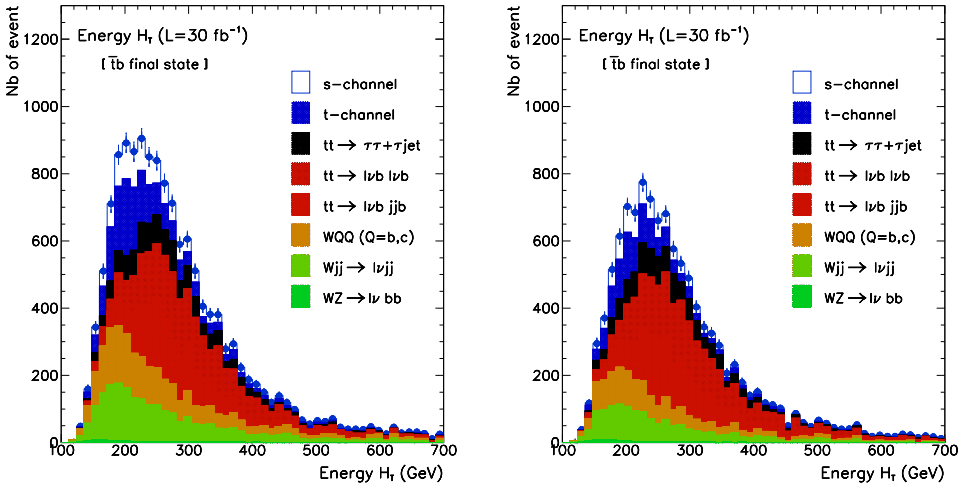

Figure 16: *Total transverse energy distribution for signal and backgrounds for 30 fb^{-1}.*

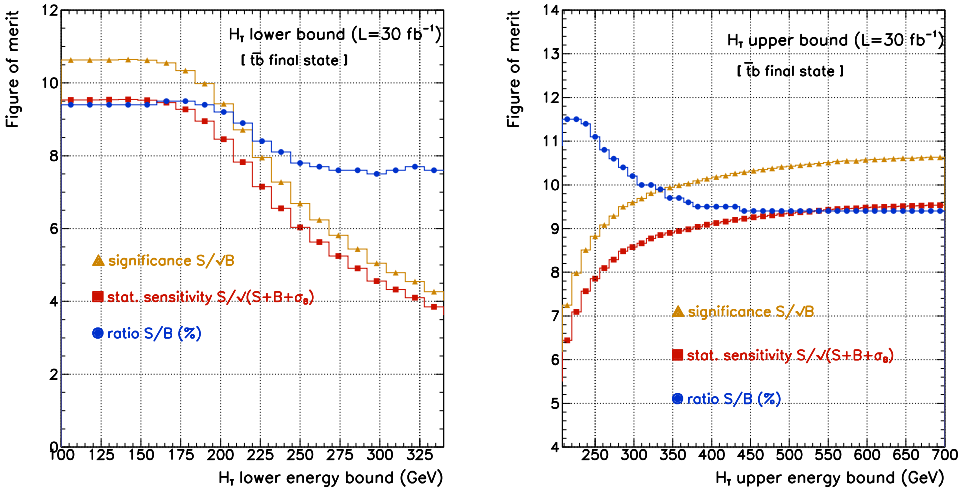

Figure 17: *Optimization for the H_T lower (left) and higher (right) boundary: are shown the ratio S/B, statistical significance and the sensitivity as s function of the lower threshold value.*

The optimal choice for the window results from a compromise between a minimal loss in statistical sensitivity and a maximal improvement in the purity: the lower threshold is set at 170 GeV/c while the upper bound is set at 300 GeV/c . The signal efficiency is decreased by about 40% for the signal. The corresponding loss is about 50% for $t\bar{t}$ events and above 70% for $WQ\bar{Q}$ and W + jets events, resulting in a slight S/B ratio increase.

3.2.2 Reconstructed Top mass m_t

With the LHC statistics, one can consider reconstructing a top mass from its decay products in order to reduce further the non-top background contamination of the selected sample. In our case where the W-boson decays leptonically, one faces an ambiguity arising from the determination of the neutrino longitudinal momentum: while the neutrino transverse energy can be inferred from the transverse missing E_T , the longitudinal momentum is unknown. It is however possible to obtain the p_z^ν by using the W-mass as a constraint as described in Ref. [3]. The longitudinal momentum can thus be written as:

$$p_z(\pm\nu) = \frac{-b \pm \sqrt{b^2 - 4ac}}{2a}$$

where :

$$a = E^2(l) - p_z^2(l) \ , \ b = -2\left(\frac{m_W^2}{2} + \vec{p_T}(l).\vec{p_T}(\nu)\right).p_z(l)$$

and

$$c = E^2(l).p_T^2(\nu) - \left(\frac{m_W^2}{2} + \vec{p_T}(l).\vec{p_T}(\nu)\right)^2$$

Usually the twofold ambiguity is lifted by chosing the solution that gives the lowest p_z^ν. At this stage of the analysis we do not apply any selection based criterium. ne has to notice that this method may have no solution: this corresponds to events where the transverse reconstructed W mass is larger than the W boson mass due to resolution effects [15]. In this case we keep the real part of the solution, following the DØ prescription [16].

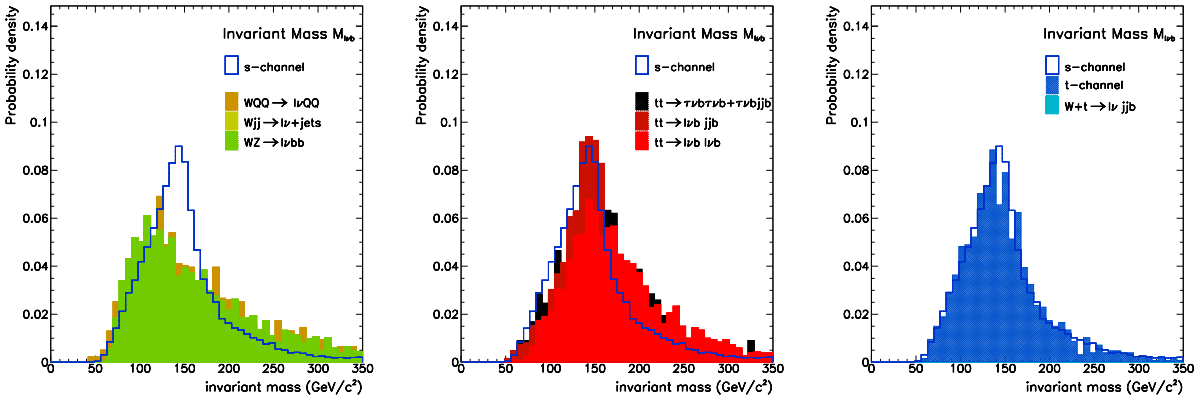

Figure 18: *Distribution of the reconstructed top mass for signal and backgrounds.*

Once the solutions to p_Z^ν are found there are four possible combinations to reconstruct the top quark momentum and mass: two depending on the neutrino solution and two due to the presence of the b-tagged jets. We choose to keep the solution leading to the highest p_T top [18]. Figs. 18 show the probability density distributions associated to the reconstructed top mass for signal

and the various backgrounds. Fig. 19 shows the event yields corresponding to an integrated luminosity of 30 fb^{-1}in the $t\bar{b}$ and $\bar{t}b$ final states.

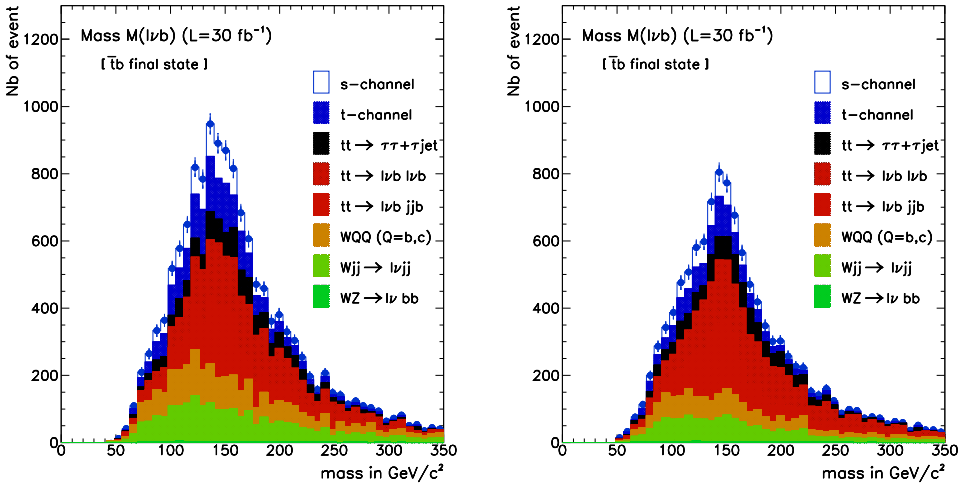

Figure 19: *reconstructed top mass for signal and backgrounds for 30 fb^{-1} for the* $t\bar{b}$ *(left) and* $\bar{t}b$ *(right) final states.*

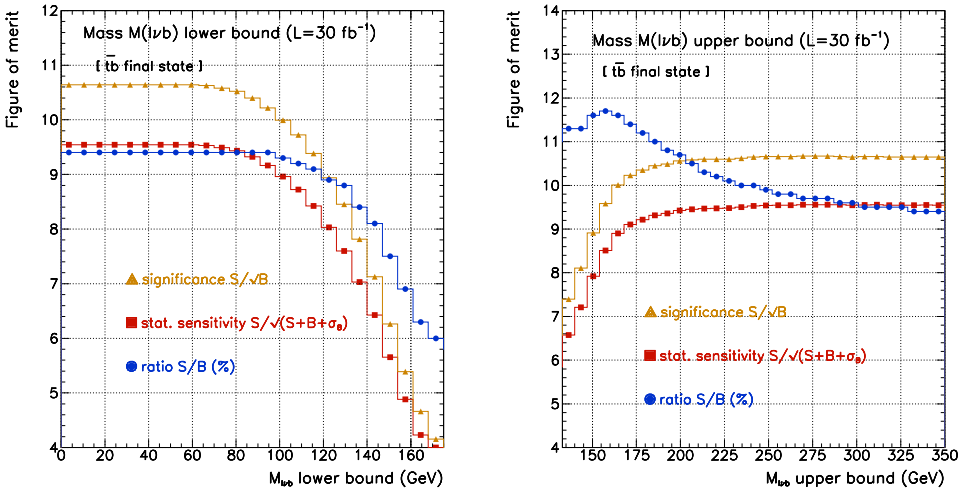

Figure 20: *Optimization for the reconstructed top mass for the lower (left) and higher (right) boundary: are shown the ratio S/B, statistical significance and the sensitivity as a function of the lower threshold value*

The optimization of the lowest and upper bounds has been performed in the same way as for the H_T quantity. Fig. 20 shows the sensitivity as a function of the M(lνb) cut respectively for the lower and the upper bounds. The choice of a reconstructed mass in the $[120, 200]$ GeV/c^2 range increases the ration S/B by 40% to about 14% at the loss of half the acceptance in signal efficiency.

We also estimate the top purity in our sample by using the MC truth information and comparing the true top momentum p_T^{true} and phi Φ_{top}^{true} with the corresponding reconstructed values p_T^{rec} and Φ_{top}^{rec}. Fig. 21 display the reconstructed top p_T as a function of the true top p_T , the difference in GeV/c as well as the difference in the Φ reconstruction. Defining a correct matching by: $|p_T^{rec} - p_T^{true}| \leq 20$ GeV/c and $|\Phi^{rec} - \Phi^{true}| \leq 0.4$ leads to an overall purity above 60%. Further studies on this topics are still on going in order to optimize the performance.

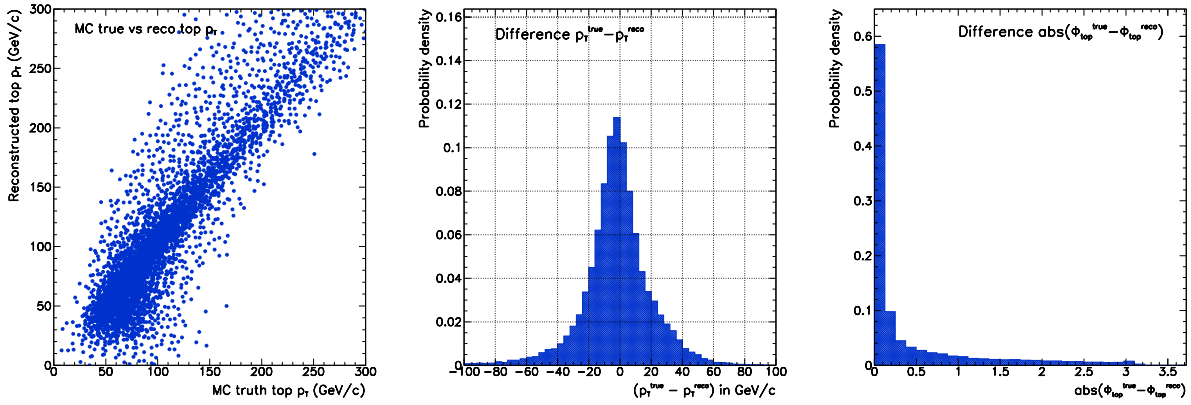

Figure 21: *Reconstructed top* p_T *as a function of the MC truth top* p_T *(left); difference between the reconstructed and true* p_T *(centre); difference in the reconstructed and true top* Φ.

processes	$t\bar{b}$ final state	$\bar{t}b$ final state
s-channel	385 ± 2	275 ± 1
t-channel	666 ± 30	410 ± 20
W+t channel	–	–
$t\bar{t}$ background		
$t\bar{t} \to e\nu b$ jjb	750 ± 35	750 ± 35
$t\bar{t} \to e\nu b$ $e\nu b$	395 ± 20	395 ± 20
$t\bar{t} \to \tau\nu b, \tau\nu b$	105 ± 7	105 ± 7
$t\bar{t} \to \tau\nu b, jjb$	20 ± 2	20 ± 2
W+jets background		
WQQ	460 ± 20	290 ± 15
$WZ \to e\nu, b\bar{b}$	18 ± 1	12 ± 1
$Wjj \to e\nu, jj$	350 ± 20	260 ± 15

Table 7: *Number of selected events in the "2b0j" sample expected for an integrated luminosity of 30* fb^{-1} *for both final states. Uncertainties come from Monte Carlo statistics only.*

3.2.3 Efficiency and statistical sensitivity

Table 7 reports the number of selected events after the H_T and the top mass criteria have been applied. The signal efficiency is reduced by 2/3 after both criteria have been applied. At the same time, non-top backgrounds are reduced by 80%. In the top pair background, the contamination from "dilepton" events is decreased by 90% while the "lepton+jet" is decreased by 70%. Note that no significant W + t events survive the topological selection.

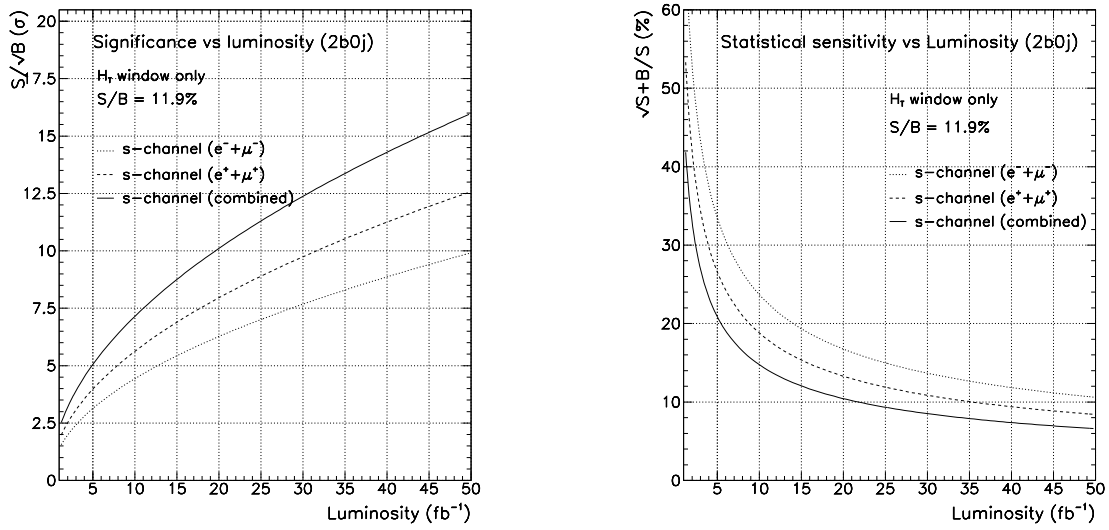

Figure 22: *Statistical significance (left) and sensitivity (right) as a function of the integrated luminosity: only the H_T requirement is applied on top plots, the full selection is applied on bottom plots.*

For the $t\bar{b}$ final state, about 385 signal events survive with 2,760 background events, resulting in an improved S/B ratio of S/B = 13.9%. For the $\bar{t}b$ final state, 275 signal events are remaining for a total background of 2,242, resulting in a S/B ratio of 12.3%. In both cases, the main background is due to the "lepton+jets" top pair production (about 30% of the total), followed by the Wg single-top (27%). Heavy flavour $WQ\bar{Q}$ events now constitute less than 20% of the remaining background, about the same order of magnitude of the W + jets background. Other top pair backgrounds (including tau decays) and WZ production are negligeable.

The statistical sensitivity to the cross-section measurement has been re-evaluated after the topological selection. It is obvious that the application of any further selection criterium resulting in a decrease of the number of expected signal events may result in a poor statistical sensitivity. Fig. 22 and Fig. 23 display the significance and statistical sensitivity as a function of the integrated luminosity in the "2b0j" sample, after the H_T window requirement only, and after the application of both H_T and m_{top} criteria.
The application of the H_T window leads to an improvement of the S/B ratio while maintaining a reasonnable high statistical sensitivity: the statistical sensitivity is below 9% with 30 fb^{-1}, while it is about 12% as the top mass requirement is used.

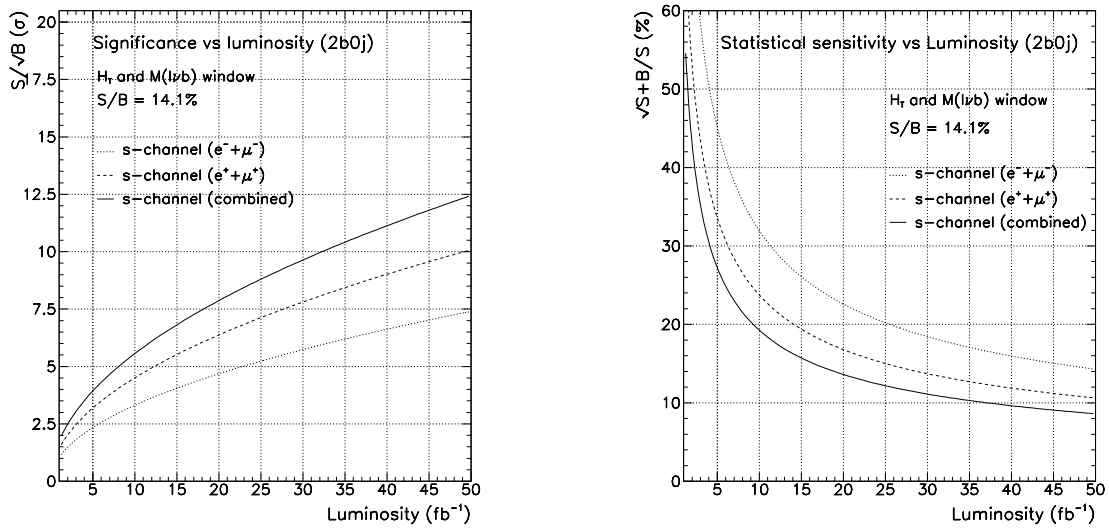

Figure 23: *Statistical significance (left) and sensitivity (right) as a function of the integrated luminosity after the full selection.*

3.3 Systematic uncertainties

The cross-section is obtained from the measurement of the total number of events passing the selection criteria minus the background estimate:

$$\sigma_{W*} = \frac{N_{obs} - N_{bckgd}}{\epsilon_{W*} \times \mathcal{L}}$$

We separate the systematic uncertainties in three different categories: the systematic uncertainties coming from the experimental biases that affect the selection efficiency for both signal and backgrounds; the uncertainty that affects specifically the background estimates, which depend on the method used to compute the individual background's contribution; the systematics due to the determination of the integrated luminosity $\mathcal{L}$. In the following we do not address the uncertainty due to the luminosity.

3.3.1 Experimental systematics common to signal and background

Common experimental systematic uncertainties originate from three main sources: the determination of the jet energy scale, the imperfect knowledge of the b-tagging efficiency and mistag rates, and the modelling of initial and final state radiations (ISR and FSR).

Jet energy scale

An uncertainty in the jet energy scale affects all jet p_T distributions, which results in a bias in the jet selection efficiency. This also has a significant impact on the jet veto performance, the determination of the missing energy as well as in the performance of the H_T and M(lνb) criteria that are used in the topological selection.

In order to quantify such effect, the energy of each jet has been shifted up and down in the Monte Carlo by a value corresponding to the jet p_T uncertainty, and half of the difference in the selection efficiency was taken as a systematic uncertainty.
Table 8 reports the variation seen as we vary the jet energy scale. A variation of 3.1% is measured in the signal efficiency ϵ_{W*}, resulting in a relative error of $\pm 1.6\%$ due to the uncertainty of the jet energy scale. For the background processes, this effect is shown to have a poor impact on to the top pair production. On the other hand, the rejection of W+jets events, which contain softer jets, depends significantly from the knowledge of the jet energy scale. A total background variation of 6.8% is measured, thus resulting in a systematic uncertainty of 3.4%.

	Number of events in 1 fb^{-1}		
processes	No scaling	$E_{jet} + \sigma_{jet}$	$E_{jet} - \sigma_{jet}$
Wg channel	22.2	24.1	20.4
$t\bar{t}$ "lepton+jets"	25.1	22.8	24.8
$t\bar{t}$ dilepton	13.1	12.7	13.4
$t\bar{t}$ ditau,tau+jets	4.2	4.5	4.2
$WQ\bar{Q}$	15.4	15.5	12.9
Wjj	11.7	11.7	9.8
Total Background	91.7	91.3	85.5
Signal	12.8	13.0	12.4

Table 8: *Number of selected events after the application of the full topological selection with the effect of a jet energy scale change.*

The magnitude of systematics effects depend on the set of selection cuts and hence may vary with the stage of the selection that is considered. Systematics are slightly higher at the preselection stage and after the application of the H_T requirement only: the effect on signal events is 5.9% after the preselection and 4.9% at the latter stage. For backgrounds, those numbers range between 5.4% and 4.5%, significantly higher than after the full selection.

b-tagging efficiency

Another source of systematics comes from the imperfect knowledge of the b-tagging efficiency and mistag rates. As can be inferred from the selection described in Section 3.1.1 b-tagging performance is crucial for background rejection. A variation of b-tagging efficiency thus directly results in a variation of the relative contribution of each sample.
Table 9 reports the variation of the number of selected events for a 55%, 60% and 65% b-tagging efficiency. Fig. 24 displays the selection efficiency as a function of the b-tagging efficiency, which shows a similar behaviour against a b-tag efficiency change for signal and backgrounds. For

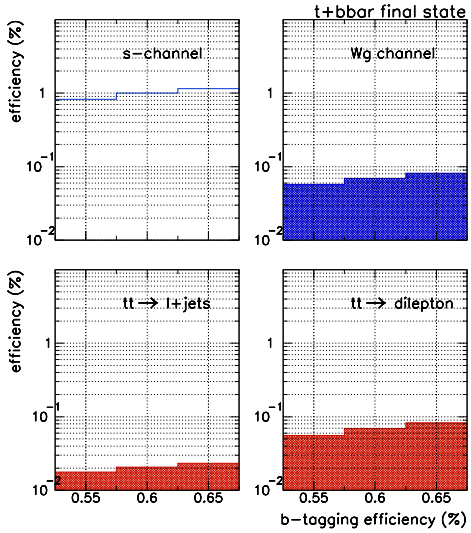

Figure 24: *Effect of b-tag efficiency on the selection efficiency for signal and three backgrounds.*

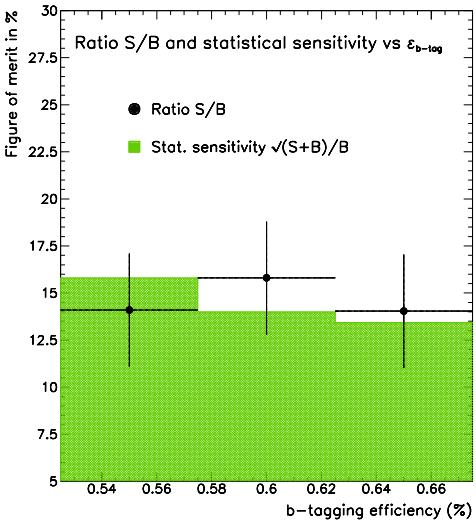

Figure 25: *Ratio S/B and statistical sensitivity as a function of b-tag efficiency.*

signal events a 3.1% change in the selection efficiency is seen for a 1% variation of the b-tagging efficiency. This change is similar for most backgrounds, with a variation of 3.2% for the summed backgrounds. This results in a relatively stable S/B ratio over the full range of variation of ϵ_b, as shown in Fig. 25.

	Number of events in 1 fb^{-1}		
processes	$\epsilon_b = 60\%$	$\epsilon_b = 55\%$	$\epsilon_b = 65\%$
Wg channel	22.2	18.5	26.0
$t\bar{t}$ "lepton+jets"	25.1	21.4	28.3
$t\bar{t}$ dilepton	13.1	10.6	15.7
$t\bar{t}$ ditau,tau+jets	4.2	3.5	5.2
$WQ\bar{Q}$	15.4	12.9	18.2
Wjj	11.7	9.8	13.7
Total Background	91.7	76.7	107.1
Signal	12.8	10.8	15.0

Table 9: *Number of selected events after the application of the full topological selection with the effect of a b-tagging variation.*

An overall uncertainty of 2% in the b-tag efficiency thus results in a relative uncertainty of 6.4% in the selection efficiency for signal and 6.6% for background.

ISR/FSR modelling

Another source of uncertainty is the modelling of initial and final gluon radiations. ISR dramatically affects the jet multiplicity of the event, while uncertainty in the FSR modelling affects the determination of the jet energy scale, which may result in a change of the selection efficiency. This is illustrated by Fig. 26 which shows the jet multiplicity for signal and background events with ISR and FSR alternatively switched ON and OFF. For b-jets the effects are particularly significant in the WQ$\bar{\text{Q}}$ selection, as seen in Fig. 27. We quantified this effect by switching ON and OFF the ISR and the FSR separately, and by considering 10% of the observed shift in the selection efficiency as a systematic error. This value constitutes a conservative approach and corresponds to the expected precision on the strong coupling constant α_s determination at the LHC [19].

	Number of events in 1 fb^{-1}		
processes	ISR/FSR on	No ISR	No FSR
Wg channel	22.2	27.9	32.8
$t\bar{t}$ "lepton+jets"	25.1	51.2	15.2
$t\bar{t}$ dilepton	13.1	27.0	16.7
$t\bar{t}$ ditau,tau+jets	4.2	8.3	3.0
WQ$\bar{\text{Q}}$	15.4	19.5	34.6
Wjj	11.7	15.0	26.0
Total Background	91.7	148.9	128.3
Signal	12.8	19.1	20.8

Table 10: *Number of selected events after the application of the full topological selection with the effect of ISR/FSR.*

Table 10 reports the number of events after the full topological selection with the ISR and FSR alternatively switched ON and OFF for signal and background. For the signal events selection, a relative variation of 4.9% is seen for the ISR alone while an effect of 6.0% is observed for the FSR. We thus quote an error of 7.7% as the quadratic sum of both effects. Backgrounds are differently affected by the ISR/FSR modelling. Top pair contributions are increased as the ISR is switched OFF because of the increased population of 2-jet events. On the other hand, as the FSR is switched OFF, most of those processes are significantly more reduced than it is the case for signal events. WQ$\bar{\text{Q}}$ events selection is particularly sensitive to FSR modelling: switching OFF the FSR tends to increase the jet energies which results in an increased jet selection efficiency. In this particular case, variations that may reach 20% are oberved in the WQ$\bar{\text{Q}}$ selection efficiency. The total effect on the sum of all backgrounds is estimated as the quadratic sum of both ISR and FSR effects. An uncertainty of 7.3% is estimated for the total background.

Systematic effects appear to affect even more the efficiency at the earlier stages of the selection.

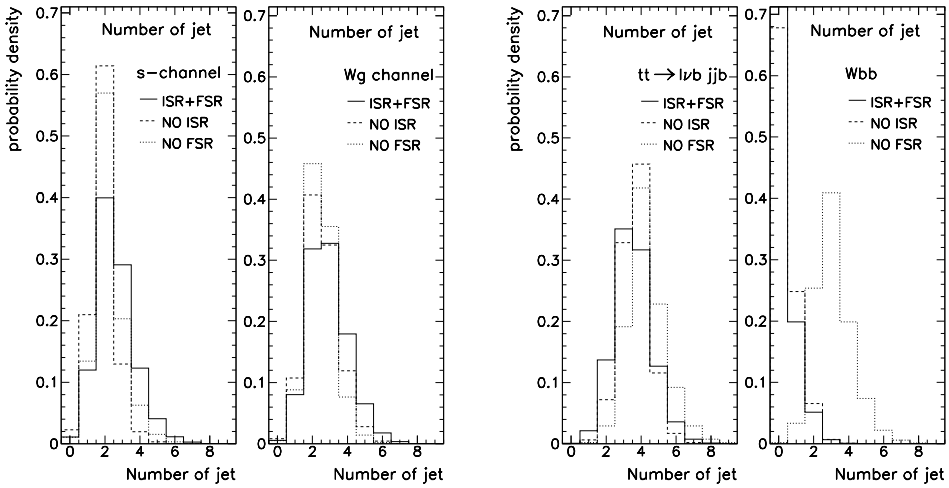

Figure 26: *Impact of ISR and FSR on jet multiplicity for s- and Wg single-top channels (on left)and for top pair and WQQ productions(right).*

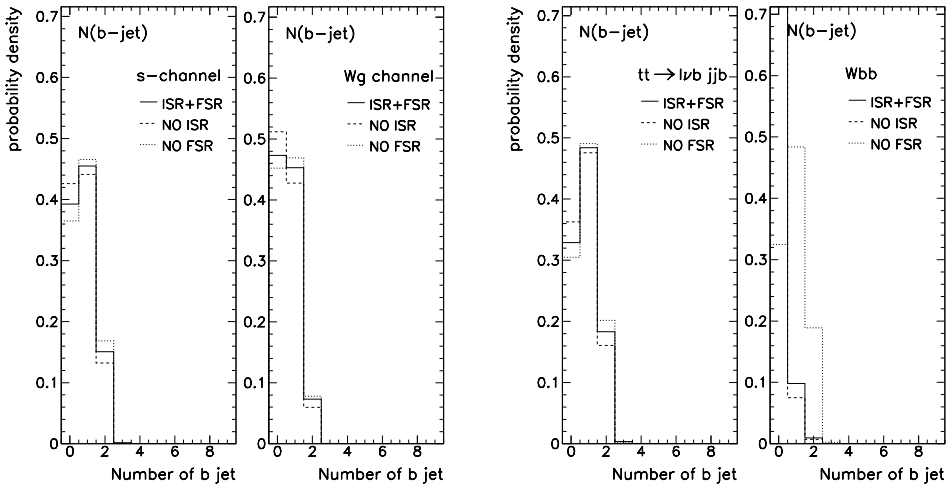

Figure 27: *Impact of ISR and FSR on jet multiplicity for s- and Wg single-top channels and for top pair and WQQ productions(right).*

For signal, the effect associated to the ISR/FSR modelling is 8.7% after the pre-selection and slightly reduced to 8% with the H_T requirement. For background, significant differences are seen in top pair and W+jets productions, as expected from Fig. 26 and Fig. 27. An uncertainty of 11.8% is quoted at the pre-selection stage and is reduced down to 9.1% as the H_T window is applied. The use of the topological selection thus helps reducing the magnitude of these effects by cutting off events in distribution tails.

Total experimental systematics

The total systematic uncertainty affecting the selection is obtained as the quadratic sum of the three effects mentionned previously. A total error of

$$\delta\epsilon_{W*}/\epsilon_{W*} = 10.3\% \text{ (systematic)}$$

is thus obtained for the signal. For the sum of all background contributions, the total systematic error is 10.4%. The level of the systematic uncertainty is thus about the same order of the statistical sensitivity.

The systematics are completely dominated by the ISR/FSR modelling effects because of the importance of the jet multiplicity requirement in the selection: a 5% relative error in the ISR/FSR would result in a total experimental systematics of 10%. The other significant effect comes from the knowledge of the b-tag and mistag rates, since the double-tag also constitute a central point in the selection. Table 11 reports the relative systematic uncertainties affecting the selection at different stages of the analysis.

	Sources of experimental systematics				Statistics
	jet E scale	b-tagging	ISR/FSR	Total	
Pre-selection	5.4%	6.4%	11.8%	14.5%	7%
HT-requirement	4.5%	6.2%	9.1%	11.8%	9%
Mtop-requirement	3.4%	6.2%	7.3%	10.1%	12%

Table 11: *Experimental systematic uncertainties at different stages of the selection.*

3.3.2 Systematics specific to the background estimates

All of the background yields rely upon Monte Carlo that are used to compute the selection efficiencies. Those generators employ LO matrix element for the hard parton scattering followed by parton showering to simulate radiation and fragmentation. We use in our cases PYTHIA v6.2, TopRex v4.1 and HERWIG v6.4 for the event generation, and normalized the event yields to the NLO cross-section, as mentionned in Section 2.2. However, even at NLO the theoretical sources of uncertainty are significant. As a consequence, direct measurements from data itself will be required.

processes	Total theoretical error
W* channel	5.0%
Wg channel	3.8%
$t\bar{t}$ production	6.2%
$Wb\bar{b}$ production	9.0%
Wjj production	15.0%

Table 12: *Theoretical systematic uncertainties used in the analysis for signal and the main backgrounds.*

The sources of theoretical uncertainties have been presented in Section 2.2. They are due to the choice of the renomalization and factorization scales, which affect the production cross-sections. Another one comes from the uncertainty associated to the choice of the parton distribution functions, that may result in a change in selection efficiencies. Finally, the uncertainty in the input top mass significantly affects both the top production cross-sections prediction. The production cross-section is expected to decrease with the top mass value: a 10% effect is indeed seen in the W* and the $t\bar{t}$ samples as the top mass input is varied from 175 GeV/c^2 to 180 GeV/c^2 . Wg and $W+t$ are less affected with a 5% decrease for the same values. Cross-section variations are shown in Fig. 28.

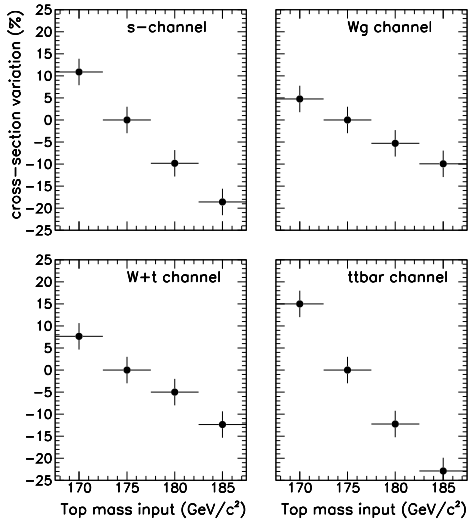

Figure 28: *Variation of the production cross-sections as a function of the input Top quark mass.*

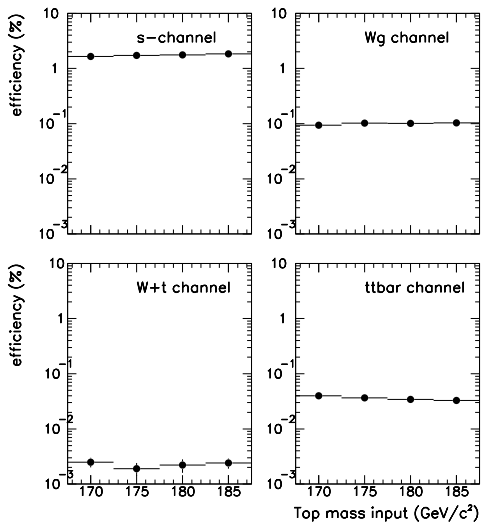

Figure 29: *Variation of the selection efficiency as a function of the input top quark mass.*

The total theoretical uncertainties on the backgrounds are reported in Table 12. A total theoretical error of 8% is quoted. Note that the input top mass also has an impact in the selection

efficiencies determination, the jet p_T distributions depending upon the mass of the decaying particle. For a higher top mass value, jet p_T distributions are shifted towards higher values, leading to a better pre-selection efficiency for all top events production: an effect of about 2% is seen in the selection efficiency of W^* and $W + t$ channels as one goes from 175 to 180 GeV/c^2 . This appears negligible in regards to other systematics.

3.4 Expected performance on the cross-section

The precision on the cross-section has been assessed for an integrated luminosity of 30 fb^{-1}at different stages of the analysis. After the simple preselection stage, results show a good statistical sensitivity but higher level of systematic uncertainties:

$$\frac{\Delta\sigma}{\sigma} = 7\%_{\text{stat}} \pm 14.5\%_{\text{exp}} \pm 8\%_{\text{bckgd theo}} \pm 5\%_{\text{lumi}}$$

The use of the H_T requirement alone in the topological selection brings some reduced sensitivity to systematic biases on a higher-purity sample:

$$\frac{\Delta\sigma}{\sigma} = 9\%_{\text{stat}} \pm 11.8\%_{\text{exp}} \pm 8\%_{\text{bckgd theo}} \pm 5\%_{\text{lumi}}$$

Using both the H_T and reconstructed top mass results in a significantly reduced level of systematics at the price of a loss in statistical sensitivity:

$$\frac{\Delta\sigma}{\sigma} = 12\%_{\text{stat}} \pm 10.1\%_{\text{exp}} \pm 8\%_{\text{bckgd theo}} \pm 5\%_{\text{lumi}}$$

In all cases, systematic errors are expected to dominate the cross-section determination. Experimental effects are dominated by the ISR/FSR modelling effects because of the importance of the jet multiplicity requirement in the selection. The other significant effect comes from the knowledge of the b-tag and mistag rates, since the double-tag also constitutes a central point in the selection. Theoretical uncertainties are the same order of magnitude of the statistical errors. They are reducible as we may be able to estimate the background contamination directly from the data. The uncertainty in the structure functions should also be reduced by some constraints from the W leptonic asymmetry measurement.

4 S-channel cross-section : interpretation in 2HDM models

The determination of the single-top s-channel cross-section is very sensitive to any new charged boson present in the underlying model. Any deviation from the Standard Model prediction may indeed be interpreted as the sign of a new (charged) heavy boson, like the charged Higgs predicted in some Two Higgs doublet models [20].

4.1 Charged Higgs production in MSSM

In 2 Higgs Doublet Models, two Higgs fields are assumed to generate the electro-weak symmetry breaking. This results into five physical states associated each to a Higgs boson: three neutral (h, H and A) and two charged bosons (H^+, H^-). In SUSY, Higgs mass spectra are predicted and depend upon one mass, usually m_A, and the $\tan\beta$ parameter, defined as the ratio of the two vacuum expectation values (vev) for the higgs fields. The allowed regions for all Higgses are shown in Fig. 30.

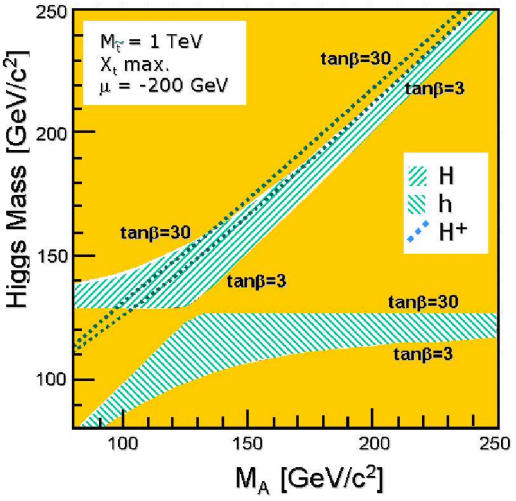

Figure 30: *Allowed region for all 5 Higgses as predicted in the MSSM in the (m_A, m_H) plane. Charged Higgs appears in dashed lines for two different values of $\tan\beta$ as a function of m_A.*

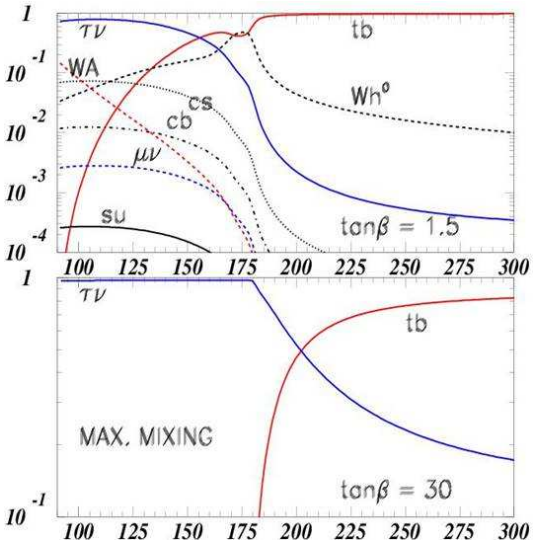

Figure 31: *Branching ratios of the charged Higgs to standard fermions and bosons as a function of the Higgs mass and for $\tan\beta = 1.5$ and $\tan\beta = 30$ as predicted in the MSSM model.*

The magnitude of the Branching ratio for the charged Higgs to the known fermions and bosons is shown in Fig. 31 as a function of its mass and for various values of $\tan\beta$. For $H^\pm$ bosons lighter than the top quark, the $\tau\nu$ and light jets decays are favored. In this case, a charged Higgs can be searched for in the precise measurement of the top pair production. For charged Higgs heavier than the top mass, the $H^+ \to t\bar{b}$ decay becomes dominant and the single-top s-channel becomes a competitive channel of discovery which can be combined with the associated production $gb \to Ht$, already described in Ref. [21].

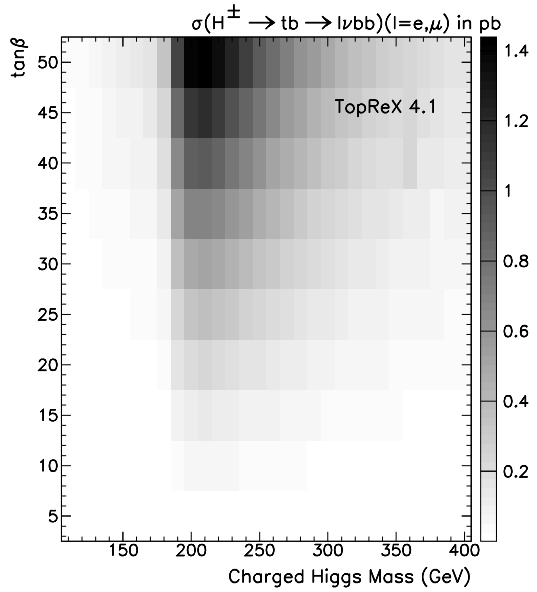

Figure 32: *Charged Higgs production cross-section $\sigma \times BR$ resulting in the $t\bar{b}$ final state using TopRex. Results are represented in the $(m_{H\pm}, \tan\beta)$ plane.*

In SUSY, the contribution to the single-top W* channel is thus expected to be enhanced due to the addition of a graph involving the $H^{\pm}$ with $H^{+} \rightarrow t\bar{b}$, resulting in a deviation from the SM expectations. As the magnitude of the $H^{+}tb$ coupling depends upon $m_{H^{\pm}}$ and $\tan\beta$, the analysis has been performed in the $(m_H, \tan\beta)$ plane. Production cross-sections are computed using the (LO) TopRex generator and are shown in Fig. 32. Those cross-sections can be as high as 2/3 of that of the W* channel for high $\tan\beta$ and Higgs masses above 200 GeV/c^2. Please note that no NLO computation was available at the time of the analysis.

4.2 Sensitivity to a charged Higgs

Selection efficiencies for Higgs events have been computed using the same selection as defined in the W* analysis including the windows on the H_T and reconstructed top mass applied in the topological selection. The total background to this Higgs signal is composed of the three single-top channels, the top pair events, the $WQ\bar{Q}$, W+jets and diboson events. Corresponding numbers are reported in Table 7. No optimization has been done to select specifically the charged Higgs boson: in particular no H_T window boundaries must be adapted according to the Higgs mass hypothesis. Numbers for efficiencies are shown in Fig. 33 in the $(m_H, \tan\beta)$ plane. The overall efficiency is of the same order of magnitude than that for the s-channel, and depends mainly on the Higgs mass, which conditions the momentum of the decaying particles. For Higgs masses well below or above the top mass, the H_T window tend to reduce the selection efficiency. The number of selected event is represented in Fig. 33 in the $(m_H, \tan\beta)$ plane, where both final states have been summed. The event yield is represented in terms of significance in Fig. 34.

We compute the significance over a fluctuation of the background estimate to which we also add systematics uncertainties of 13.7%. A 5 σ discovery seems achievable only for high $\tan\beta$

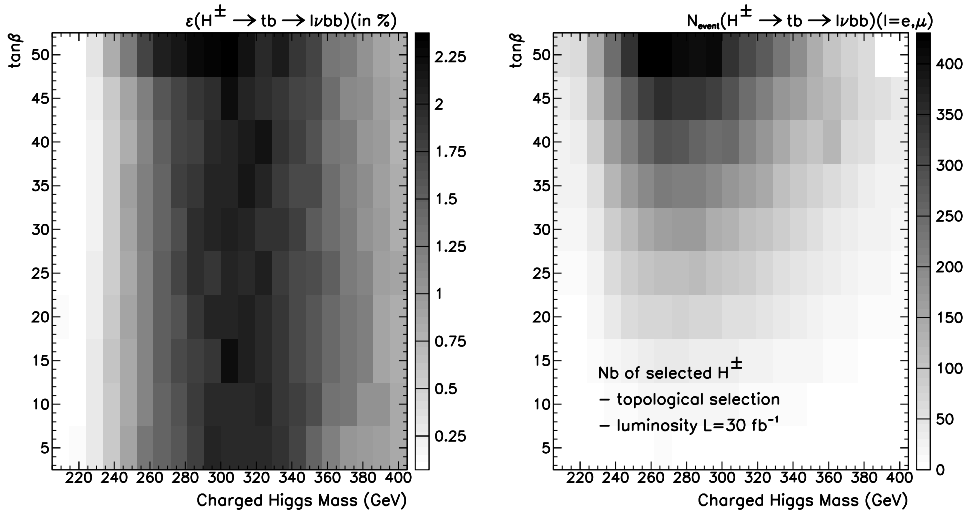

Figure 33: *(Left) Signal selection efficiency in the* $(\mathrm{m_H}, \tan\beta)$ *plane. (Right) Number of selected Higgs events in the* $(m_{H\pm}, \tan\beta)$ *plane.*

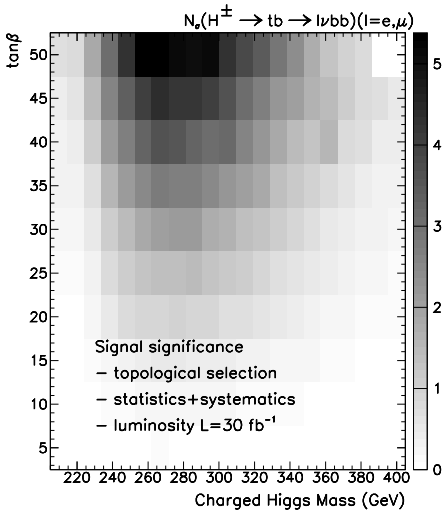

Figure 34: *Significance to a charged Higgs boson in the* $(m_H, \tan\beta)$ *plane in terms of a 5* σ *discovery, 3* σ *evidence or a 95% exclusion contours for a luminosity of 30* fb^{-1}*. Both statistical and total systematic errors (including experimental effects, theoretical effects and luminosity) have been included.*

and Higgs mass above 250 GeV/c^2. This result should be improved by using a specific selection using the specific property for the scalar $H^{\pm}$. It should also benefit from the combination with the W+t events searches.

5 Conclusion

We investigate in this report the possibility to measure the s-channel contribution to the single-top cross-section during the low luminosity period of data taking at the LHC.

A specific analysis has been developed and shows that for an integrated luminosity of 30 fb^{-1}a statistical sensitivity below 10% can be achieved (it is 12% if the full selection is applied). After a simple preselection stage based on the presence of a high p_T lepton, high mE_T and exactly two b-tagged jets, the precision on the cross-section is:

$$\frac{\Delta\sigma}{\sigma} = 7\%_{\text{stat}} \pm 14.5\%_{\text{exp}} \pm 8\%_{\text{bckgd theo}} \pm 5\%_{\text{lumi}}$$

The use of an extra requirement on the total energy H_T brings some reduced sensitivity to systematic biases a higher-purity:

$$\frac{\Delta\sigma}{\sigma} = 9\%_{\text{stat}} \pm 11.8\%_{\text{exp}} \pm 8\%_{\text{bckgd theo}} \pm 5\%_{\text{lumi}}$$

Using a topological selection based on H_T and the reconstructed top mass in the leptonic channel results in a significantly reduced level of systematics at the price of a loss in statistical sensitivity:

$$\frac{\Delta\sigma}{\sigma} = 12\%_{\text{stat}} \pm 10.1\%_{\text{exp}} \pm 8\%_{\text{bckgd theo}} \pm 5\%_{\text{lumi}}$$

This analysis also show that systematic errors are expected to dominate the measurement. Dominant errors are due to the ISR/FSR modelling and the imperfect knowledge of the b-tagging efficiency and mistag rates. This report also shows that theoretical uncertainties affecting the background estimates are of the same order of magnitude than that of the statistical errors. Thus, they may be reduced by the use of data to evaluate the background contamination. The uncertainty in the pdf which affect all samples, should also benefit from the constraints that W/Z leptonic asymmetry measurements should bring. The analysis has been developed using the fast simulation of Atlas. Further studies must be carried in order to confirm the obtained results. Besides, the analysis is based upon samples produced with LO generators: it must therefore be re-run with the relevant NLO generators as they become available.

The measurement of the s-channel contribution constitutes a powerful probe for new physics. In a 2HDM model, the coupling of a charged Higgs boson $H^{\pm}$ to the top quark can be significant in some areas of the $(m_H, \tan\beta)$ planes. Providing that we are able to measure precisely the s-channel cross-section, we have shown that this search could lead to a discovery for high values of $\tan\beta$ and for a Higgs mass above 250 GeV/c^2 in three years of data taking at low luminosity, thus complementing the direct search via the gb fusion.

6 Acknowledgements

This analysis has been performed within the ATLAS collaboration and we would like to thank the members of the "Top Physics" group for fruitful discussions. We are grateful to Antonio Onofre and the LIP group for their careful reading of this document and for many relevant comments and suggestions made on this report. Special thanks to Benoit Clement (IN2P3/IReS) for helpful discussions on the top mass reconstruction in DØ .

References

[1] M. Beneke et al., hep-ph/0003033. N. Kidonakis and R. Vogt, Phys. Rev. D68, 114014 (2003), Eur. Phys. J C33,s466 (2004)

[2] The Atlas coll., "Atlas Detector and Physics Performance" CERN/LHC/99-14 (1999)

[3] D. O'Neil PhD., "The Physics of the Electroweak top quark production in ATLAS" (1999)

[4] S. Frixione, talk at the "Atlas Top meeting" CERN, 22 Feb. 2006

[5] Z. Sullivan "Understanding single-top quark production and jets @ hadron colliders" hep-ph/0408049.

[6] J. Campbell, K. Ellis, F. Tramontano, "Single-top production and decay at NLO", hep-ph/0408158

[7] J. Campbell, F. Tramontano "NLO corrections to Wt production and decay" hep-ph/0506289

[8] TopReX generator, hep-ph/0201292.

[9] MC@NLO generator, ,S. Frixione, B. Weber, P. Nason, hep-ph/0204244 and hep-ph/0305252

[10] F. Hubaut, P. Pralavorio , hep-ex/0508061

[11] J. Campbell, K. Ellis, D. Rainwater, "NLO QCD predictions for W+2 jets and Z+2 jets production at the LHC" hep-ph/0308195

[12] Herwig generator, G. Corcella et al., hep-ph/0011363, hep-ph/0210213

[13] M. Dobbs "Incorporating NLO matrix element for hadronic diboson production in showering event generators" Phys. Rev. D64 034016

[14] ATLFAST, ATL-PHYS-98-131

[15] A. Lucotte, "Single-top cross-section measurements in ATLAS", ATLAS Rome Workshop, June 8th 2005

[16] B. Clement, IReS, private communication

[17] F. Hubaut, P. Pralavorio, "Comparison of ATLFAST and Fullsim performance", Top meeting CERN, Feb. 22nd (2005)

[18] I. Bojanovic et al., hep-ex/0403021

[19] H. Stenzel, "Determination of alpha_s using jet cross-section at hadron colliders" ATLAS-PHYS-2001-0003

[20] J.F. Gunion et al., "Higgs Hunter's Guide" (Addison-Wesley, NY, 1990); R. Santos and A. Barroso, Phys. Rev. D56 5366 (1997); V. Berger et al., Phys. Rev. D41 3421 (1990); Y. Grossman Nucl. Phys B426 355 (1994)

[21] K. Assamagan, ATL-PHYS-PUB-2005-017, SN-ATLAS-2004-042